

**Investigation of nuclear collectivity in the neutron mid-shell nucleus  $^{186}\text{Pb}$** 

J. Pakarinen,<sup>1,2,\*</sup> V. Hellemans,<sup>3</sup> R. Julin,<sup>1</sup> S. Juutinen,<sup>1</sup> K. Heyde,<sup>3</sup> P. -H. Heenen,<sup>4</sup> M. Bender,<sup>5</sup> I. G. Darby,<sup>2</sup> S. Eeckhaudt,<sup>1</sup> T. Enqvist,<sup>1,†</sup> T. Grahn,<sup>1</sup> P. T. Greenlees,<sup>1</sup> F. Johnston-Theasby,<sup>6</sup> P. Jones,<sup>1</sup> H. Kettunen,<sup>1</sup> M. Leino,<sup>1</sup> A.-P. Leppänen,<sup>1,‡</sup> P. Nieminen,<sup>1,§</sup> M. Nyman,<sup>1</sup> R. D. Page,<sup>2</sup> P. M. Raddon,<sup>6</sup> P. Rahkila,<sup>1</sup> C. Scholey,<sup>1</sup> J. Uusitalo,<sup>1</sup> and R. Wadsworth<sup>6</sup>

<sup>1</sup>*Department of Physics, University of Jyväskylä, P.O. Box 35, FI-40014, Jyväskylä, Finland*

<sup>2</sup>*Department of Physics, Oliver Lodge Laboratory, University of Liverpool, Liverpool L69 7ZE, United Kingdom*

<sup>3</sup>*Department of Subatomic and Radiation Physics, Proeftuinstraat, 86 B-9000 Gent, Belgium*

<sup>4</sup>*Dapnia/SPH, CEA Saclay, F-91191 Gif sur Yvette Cedex, France*

<sup>5</sup>*Department de Physique Nucléaire Théorique, Université Libre de Bruxelles, Case Postale 229, B-1050 Bruxelles, Belgium*

<sup>6</sup>*Department of Physics, University of York, Heslington, York YO1 5DD, United Kingdom*

(Received 17 July 2006; published 3 January 2007)

For the first time, non-yrast structures of the neutron mid-shell nucleus  $^{186}\text{Pb}$  have been identified in an in-beam  $\gamma$ -ray spectroscopy measurement using the recoil-decay tagging technique. The yrast band has been tentatively extended up to  $I^\pi = 20^+$ , revealing a similar backbend to that observed in the Pt and Hg isotones. Three new bands and several other transitions have been observed. Calculations carried out in the framework of the interacting boson model together with mean-field studies using the generator coordinate method provide arguments for the association of one of the new bands with an oblate shape. The present data also show evidence for octupole and  $\gamma$ -vibrational bands.

DOI: [10.1103/PhysRevC.75.014302](https://doi.org/10.1103/PhysRevC.75.014302)

PACS number(s): 27.70.+q, 21.10.Re, 23.20.Lv, 25.70.Gh

**I. INTRODUCTION**

The interplay between single-particle motion, collectivity, and pairing in light Pb nuclei is manifested as a rich gamut of coexisting nuclear shapes and exotic excitations [1–5]. One of the goals of modern nuclear physics research is to understand the origin of these structures and their relation to the fundamental interactions between the nuclear constituents. These subjects can be investigated particularly well in the Pb isotopes close to neutron mid-shell, where a relatively small proton shell gap, together with a large valence neutron space, provides fertile ground for studies of shape transitions within a small energy range.

The occurrence of excited  $0^+$  states in this region is generally associated with multiparticle-multihole ( $np$ - $nh$ ) proton excitations across the closed  $Z = 82$  shell [1,4]. They intrude down close to energies of the spherical ground states when approaching the neutron mid-shell at  $N = 104$  [2,6–9]. A complementary view of these  $0^+$  states is provided by mean-field methods in which each intruder minimum is associated with a different collective shape. The first calculations of quadrupole potential energy surfaces were performed within the Strutinsky approach [10–12]. The existence of a spherical ground state with low-lying oblate and prolate minima has been confirmed by self-consistent mean-field approaches based on effective

Skyrme [13–15] and Gogny [16] interactions. In a truncated shell-model approach, these oblate and prolate mean-field configurations can be associated with proton 2p-2h and 4p-4h excitations, respectively, forming a unique system of three different shapes.

Much experimental effort has been put into investigating these nuclei, but the information obtained is still rather scarce. The low-lying  $0^+$  states can be populated in the decay of parental nuclei. In 2001, Andreyev *et al.* established in an  $\alpha$ -decay fine-structure measurement of  $^{190}\text{Po}$  the triplet of  $0^+$  states in  $^{186}\text{Pb}$  [8]. Above the spherical ground state, they observed  $0^+$  states at 532 and 650 keV, which may be related to underlying proton 2p-2h and 4p-4h structures or from the collective point of view, an oblate and prolate shape, respectively.

To confirm the interpretation of these states, it would be important to measure rotational bands built on these states. Such bands can be studied using in-beam  $\gamma$ -ray spectroscopic methods employing fusion-evaporation reactions. However, such measurements are restricted by experimental difficulties as one must distinguish between  $\gamma$  rays from very rare evaporation residues and the more overwhelming background of  $\gamma$  rays from fission products. Moreover, the decay pattern favors the feeding of yrast states, non-yrast states being populated very weakly. In  $^{186}\text{Pb}$ , the yrast band was measured for the first time by Heese *et al.* [17] and almost simultaneously by Baxter *et al.* [18]. Their results were confirmed with a few new transitions by Reviol *et al.* [19]. All previous in-beam measurements were based on the observation of prompt  $\gamma$  rays in coincidence with recoils. This work presents the first recoil-decay tagged  $\gamma\gamma$ -coincidence data for  $^{186}\text{Pb}$ ; other results have been published in Refs. [20,21].

The identification of the 650 keV  $0_3^+$  state in  $^{186}\text{Pb}$  represents the only firm observation of a prolate intruder  $0^+$

\*E-mail enquiries: [jp@ns.ph.liv.ac.uk](mailto:jp@ns.ph.liv.ac.uk)

†Present address: Centre for Underground Physics, P.O. Box 22, FI-86801, Pyhäsalmi, Finland.

‡Present address: Northern Finland Regional Laboratory, STUK-Radiation and Nuclear Safety Authority, Rovaniemi, Finland.

§Present address: Department of Nuclear Physics, The Australian National University, Canberra, ACT 0200, Australia.

state in Pb isotopes [8], whereas prolate bands have been identified in five even-even  $^{182-190}\text{Pb}$  isotopes [17,18,22–24]. In the decay of these bands, the  $0^+$  band head is bypassed because of the competing high-energy  $E2$  transition from the  $2^+$  band member to the spherical ground state. Prolate yrast bands, very similar to those in these Pb isotopes, have also been observed in even-mass Hg and Pt isotopes with  $100 \leq N \leq 108$  [1,5] and recently in  $^{190}\text{Po}$  [25]. Yrast bands associated with oblate intruder structures have been observed in  $^{192}\text{Po}$ ,  $^{194}\text{Po}$  [5], and  $^{198}\text{Rn}$  [26].

This paper is organized as follows: In Sec. II, the experimental procedure is described; in Sec. III, the analysis method and results are discussed; in Sec. IV, the properties of observed bands are discussed. In Sec. V, two complementary theoretical descriptions of the neutron-deficient Pb nuclei are presented. Conclusions of the present work are formulated in Sec. VI.

## II. EXPERIMENTAL DETAILS

The experiment was performed at the Accelerator Laboratory of the University of Jyväskylä. A beam of  $^{83}\text{Kr}^{16+}$  ions was accelerated in the K130 cyclotron [27] to an energy of 355 MeV and used to populate excited states of  $^{186}\text{Pb}$  via the  $^{106}\text{Pd}(^{83}\text{Kr},3n)^{186}\text{Pb}$  fusion-evaporation reaction. The  $^{106}\text{Pd}$  target was a metallic foil of thickness 1 mg/cm<sup>2</sup> and 98.5% isotopic enrichment. The beam current was limited to approximately 6 pA, yielding an average recoil counting rate of 200 Hz at the focal plane.

Prompt  $\gamma$  rays were observed using the JUROGAM array consisting of 42 Compton-suppressed Ge detectors. Detectors were distributed over six angular rings with respect to the beam direction with five at  $158^\circ$ , ten at  $134^\circ$ , ten at  $108^\circ$ , five at  $94^\circ$ , five at  $86^\circ$ , and seven at  $72^\circ$ . The total photo-peak efficiency of the JuroGam array for 1332 keV  $\gamma$  rays was 4.1%.

Fusion-evaporation residues were separated from the primary beam using the recoil ion transport unit (RITU), a gas-filled separator [28]. The transmission efficiency of the RITU for Pb residues in the present experiment was approximately 30%. The GREAT spectrometer [29] was employed at the focal plane. Implanted evaporation residues and their subsequent  $\alpha$  decays were detected by two double-sided silicon strip detectors (DSSSDs) of high granularity (4800 pixels in total). A transmission multiwire proportional counter placed upstream of the DSSSDs was used to obtain energy loss and time-of-flight information for the recoils. A box of 28 PIN diodes, also upstream of the DSSSDs, was used to detect  $\alpha$  particles which escaped from the DSSSDs. In addition, two phase I Ge detectors [30] were mounted above and behind the DSSSDs in transverse geometry to measure delayed  $\gamma$  rays from isomeric states.

Data were collected using the triggerless total data readout (TDR) data acquisition system [31]. In TDR, each channel is run independently and associated via software with data words. Each data word is time stamped with a global 100 MHz clock and passed to the event builder for event reconstruction. The only dead time arises from the analog shaping and conversion times of signals in the individual channels. The temporal

and spatial correlations of the data were performed using the GRAIN software package [32].

Prompt  $\gamma$  rays correlated with the subsequent  $\alpha$  decay of a  $^{186}\text{Pb}$  recoil within 15 s in the same pixel of the DSSSD were selected in the data analysis. During 151 h of beam time, approximately  $10^6$   $\alpha$  particles from  $^{186}\text{Pb}$ , including escape events, were recorded. This resulted in  $6 \times 10^5$  recoil-gated  $\alpha$ -tagged prompt  $\gamma\gamma$ -coincidence events associated with  $^{186}\text{Pb}$ . The  $\gamma\gamma$ -coincidence analysis was finalized using the RADWARE software package [33]. The cross section for  $^{186}\text{Pb}$  was estimated to be 185  $\mu\text{b}$ . Such studies have so far been difficult because of the low production cross section and relatively long half-life of  $^{186}\text{Pb}$  (4.83 s [34]).

## III. RESULTS

The high efficiency of the JuroGam Ge-detector array enabled the collection of sufficient recoil-decay tagged  $\gamma\gamma$ -coincidence events to place a large number of new transitions into a level scheme. Due to the long  $\alpha$ -decay searching time, random correlations from the  $^{186,187}\text{Tl}$  and  $^{184,186}\text{Hg}$  nuclei gave rise to contaminant peaks in  $\gamma$ -ray spectra (contaminant level approximately 2% for each major contaminant nucleus). This made the  $\gamma\gamma$ -coincidence analysis more complicated as several  $\gamma$  rays originating from these nuclei overlapped with  $\gamma$ -ray energies of transitions in  $^{186}\text{Pb}$ .

Transitions associated with  $^{186}\text{Pb}$  are listed in Table I. The level scheme deduced for  $^{186}\text{Pb}$ , incorporating over 20 new states and more than 30 new  $\gamma$  rays, is shown in Fig. 1. The scheme was constructed using the coincidence relations and intensity balances in the recoil-gated,  $\alpha$ -tagged  $\gamma\gamma$ -coincidence data.

In the present work, multipolarities of some transitions could be deduced from the angular distributions  $A_2/A_0$  [35,36] and intensity ratios of  $\gamma$  rays ( $R$ ) [37]. These values are listed in Table I when available. Deduced values for  $A_2/A_0$  and  $R$  were compared with theoretical predictions and with the values deduced for the known transitions of different multipolarities. For a known stretched  $E2(25/2^+ \rightarrow 21/2^+)$  transition in  $^{187}\text{Tl}$ , a ratio  $R$  of 1.2(2) was observed, while for a dipole  $11/2^- \rightarrow 9/2^-$  transition in  $^{185}\text{Tl}$ , the corresponding value was 0.6(2). These ratios are in accord with the theoretical predictions of 1.45 and 0.73, respectively. For an  $E2(6^+ \rightarrow 6^+)$  transition, theory predicts an  $A_2/A_0$  ratio of  $-0.15$ , whereas for  $R$  (at angles between  $157.60^\circ$  and  $85.84^\circ + 94.16^\circ$ ), it gives a ratio of 0.82. The corresponding values for an  $M1(6^+ \rightarrow 6^+)$  transition are 0.39 and 1.60, respectively.

Because of the deorientation of recoiling ions [38] (recoil-in-vacuum effect) and overlapping transition energies, information concerning the spin assignments from the  $\gamma$ -ray angular distributions was difficult to obtain, especially at low spin.

### A. Band I

The yrast  $E2$  cascade in  $^{186}\text{Pb}$  has recently been observed up to  $I^\pi = 14^+$ , where the  $I^\pi = 12^+$  and  $I^\pi = 14^+$  states were tentatively assigned [19]. In the present work, this cascade is

TABLE I.  $\gamma$ -ray transitions measured for  $^{186}\text{Pb}$  in the present work.  $\gamma$ -ray energy ( $E_\gamma$ ), relative  $\gamma$ -ray intensity ( $I_{\text{rel}}$ ) normalized to 1000 for the  $2_1^+ \rightarrow 0_1^+$  transition, level energy ( $E_i$ ), (tentatively) assigned spin and parity of the initial and final levels ( $I_i^\pi$  and  $I_f^\pi$ ), and angular distribution information ( $A_2/A_0$  and  $R$ ) are listed. For the weakest  $\gamma$ -ray transitions, only the intensity limits are given.

$E_\gamma$ (keV)	$I_{\text{rel}}$	$E_i$ (keV)	$I_i^\pi$	$I_f^\pi$	$A_2/A_0$	$R$
260.6(1)	790(80)	923(1)	$4_1^+$	$2_1^+$	-0.08(4)	0.9(2)
306(2)	<5	2593(1)	$(9_1^-)$	$(7_1^-)$		
307(2)	<6	1644(1)	$(5_1^+)$	$(4_2^+)$		
337(1)	<7	1644(1)	$(5_1^+)$	$(3_1^+)$		
337.1(1)	740(70)	1260(1)	$6_1^+$	$4_1^+$	-0.02(3)	1.1(2)
361.8(5)	9(4)	1307(1)	$(3_1^+)$	$(2_2^+)$		
369.1(4)	9(3)	2962(1)	$(11_1^-)$	$(9_1^-)$		
384(4)	11(5)	1307(1) or 1644(1)	$(3_1^+)$ or $(5_1^+)$	$4_1^+$ or $6_1^+$		
391.5(2)	40(7)	1337(1)	$(4_2^+)$	$(2_2^+)$	-0.1(2)	0.9(4)
401.3(2)	55(7)	1738(1)	$(6_2^+)$	$(4_2^+)$		1.1(3)
405.3(6)	7(3)	2049(1)	$(7_1^+)$	$(5_1^+)$		
414.5(5)	21(7)	1337(1)	$(4_2^+)$	$4_1^+$		
414.8(1)	560(50)	1675(1)	$8_1^+$	$6_1^+$		
419.5(3)	4(3)	3381(1)	$(13_1^-)$	$(11_1^-)$		
424.1(2)	42(5)	2163(1)	$(8_2^+)$	$(6_2^+)$	0.15(5)	1.5(1.0)
461.3(7)	11(3)	3843(2)	$(15_1^-)$	$(13_1^-)$		
462.7(2)	39(5)	2625(1)	$(10_2^+)$	$(8_2^+)$		
469.5(4)	16(4)	2519(1)	$(9_1^+)$	$(7_1^+)$		
478.8(2)	38(5)	1738(1)	$(6_2^+)$	$6_1^+$	-0.2(2)	0.6(3)
485.8(5)	280(30)	2160(1)	$10_1^+$	$8_1^+$	0.08(7)	1.4(4)
487.4(4)	23(6)	2163(1)	$(8_2^+)$	$8_1^+$		
498.4(7)	<2	4341(2)	$(17_1^-)$	$(15_1^-)$		
507.6(3)	18(3)	3133(1)	$(12_2^+)$	$(10_2^+)$		
527(1)	<4	3046(2)	$(11_1^+)$	$(9_1^+)$		
543(1)	<3	3409(2)				
549.6(6)	134(9)	2710(1)	$12_1^+$	$10_1^+$	0.16(9)	1.3(4)
551.3(9)	5(3)	3684(2)	$(14_2^+)$	$(12_2^+)$		
605.6(8)	71(5)	3316(1)	$(14_1^+)$	$12_1^+$		
645(1)	<5	1307(1)				
652.2(5)	22(2)	3968(2)	$(16_1^+)$	$(14_1^+)$		
662.2(2)	1000(60)	662(1)	$2_1^+$	$0_1^+$	-0.04(2)	1.0(2)
668(2)	<10	4635(4)	$(18_1^+)$	$(16_1^+)$		
673(1)	<5	5308(4)	$(20_1^+)$	$(18_1^+)$		
674.5(6)	14(5)	1337(1)	$(4_2^+)$	$2_1^+$	0.05(13)	
705.5(4)	<3	2866(1)	$(3_1^+)$	$2_1^+$		
720(2)	19(6)	1644(1)	$(5_1^+)$	$(4_1^+)$	-0.07(15)	
750(3)	<3					
770(3)	<3					
790(4)	9(4)	2049(1)	$(7_1^+)$	$(6_1^+)$		
801.2(5)	10(3)	2962(1)	$(11_1^-)$	$(10_1^+)$		
837(2)	<4					
844(3)	<3	2519(1)	$(9_1^+)$	$(8_1^+)$		
867(3)	<4					
918.1(3)	12(4)	2593(1)	$(9_1^-)$	$(8_1^+)$	-0.3(2)	
945.2(3)	51(6)	945(1)	$(2_2^+)$	$0_1^+$	0.0(2)	1.0(4)
1027(2)	10(5)	2287(1)			-0.2(3)	
1043(3)	<3					
1112(3)	<5					
1207(4)	<10				-0.1(3)	

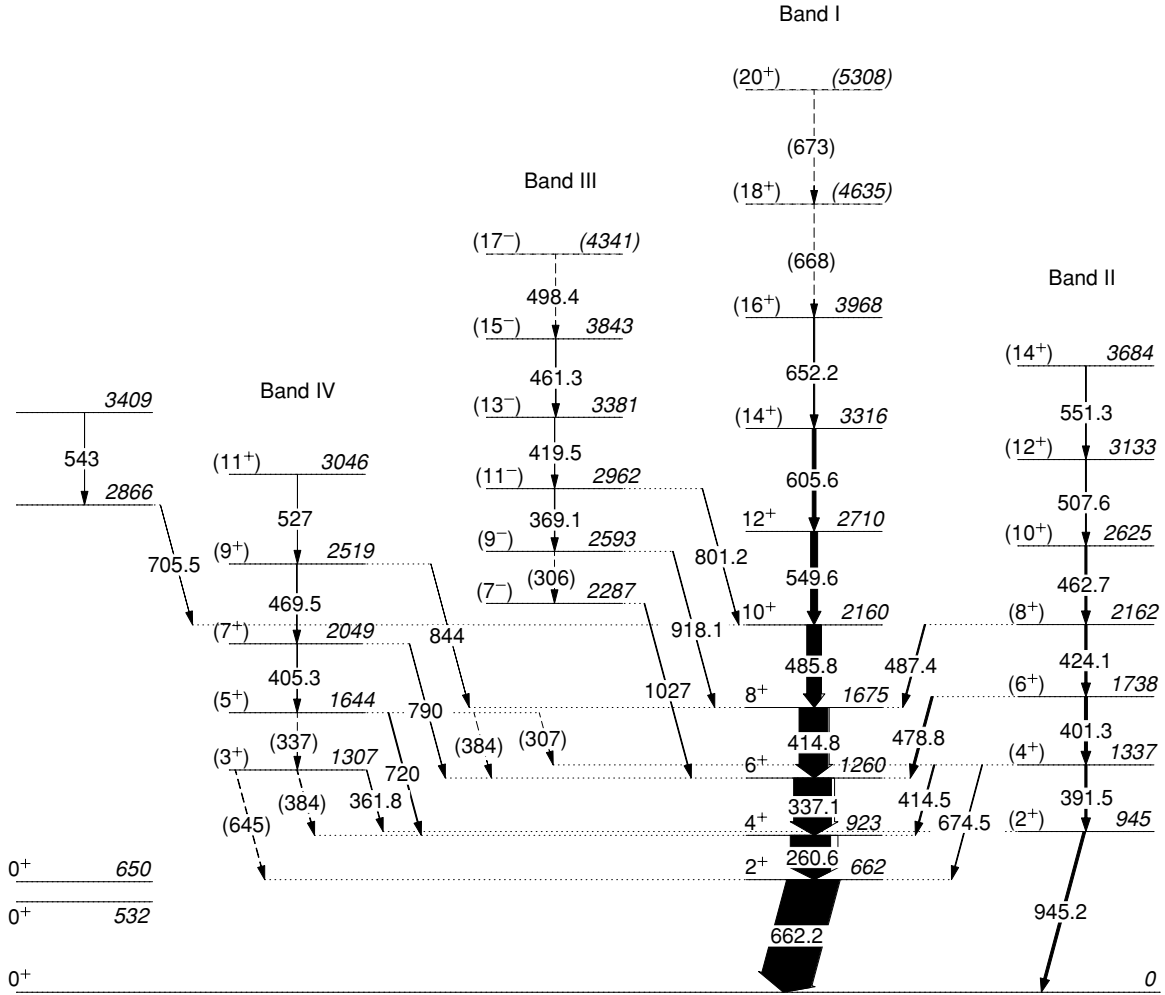


FIG. 1. Level scheme of  $^{186}\text{Pb}$  deduced from the present data (the two  $0^+$  states on the left side are taken from Ref. [8]). Bands have been named in decreasing order of their intensities.

confirmed up to  $I^\pi = 10^+$ , and the 2710 keV level is assigned with  $I^\pi = 12^+$ , as the 550 keV transition has the angular distribution ratio of a stretched  $E2$ . The  $14^+ \rightarrow 12^+$  transition was measured to have an energy 4 keV higher than that reported in Ref. [18] and 10 keV higher than that in Ref. [19].

Figure 2(a) shows background-subtracted recoil-gated  $\alpha$ -tagged  $\gamma\gamma$ -coincidence spectrum. In addition to previously known yrast-band transitions, it also reveals peaks with energies around 400 keV. The 945 keV transition feeding the  $0^+$  ground state (see Sec. III B) has been marked.

The spectrum shown in Fig. 2(b) was gated by the highest yrast-band transition of 550 keV observed firmly by Reviol *et al.* [19]. In the inset, the energy range between 640 and 690 keV is magnified. The known and the new yrast-band transitions have been marked with corresponding  $\gamma$ -ray energies.

Figure 2(c) shows a sum of spectra gated on the 606, 652, and 668 keV transitions, revealing the whole yrast cascade observed in the present work. The tentative spin assignments for the two highest yrast-band levels were based on the assumption of the persistence of the rotational band and on the transition energies and intensities. Consequently, the

$\gamma\gamma$ -coincidence data reveal candidates for the extension of the yrast band up to  $I^\pi = 20^+$ . Where the next transition would lie is highly speculative, but candidates are at 703 or 723 keV. In the inset, a part of the spectrum is again magnified.

### B. Band II

Figure 3(a) presents a recoil-gated,  $\alpha$ -tagged  $\gamma\gamma$ -coincidence spectrum gated by the 945 keV transition. Since no coincidences with the yrast-band transitions can be seen, the gating transition must be above an isomeric state or feed the ground state. The former is excluded by means of similar gates on the feeding transitions, which are in coincidence with the yrast-band transitions. Therefore, the transition is assigned to deexcite a  $2_2^+$  state at 945 keV. This interpretation is analogous to the  $^{188}\text{Pb}$  case, where a similar  $2_2^+$  state exists at 953 keV [39]. Because of the dominant high-energy  $E2(2_2^+ \rightarrow 0_1^+)$  ground-state transition and some overlapping transitions, the  $E2(2_2^+ \rightarrow 0_2^+)$  transition to the oblate  $0^+$  state and the possible branch to the prolate  $0_3^+$  state from the  $2_2^+$  state remain unobserved in  $^{188}\text{Pb}$  and in  $^{186}\text{Pb}$ . In addition, the  $2_2^+ \rightarrow 2_1^+$  transition was not observed in  $^{186}\text{Pb}$ .

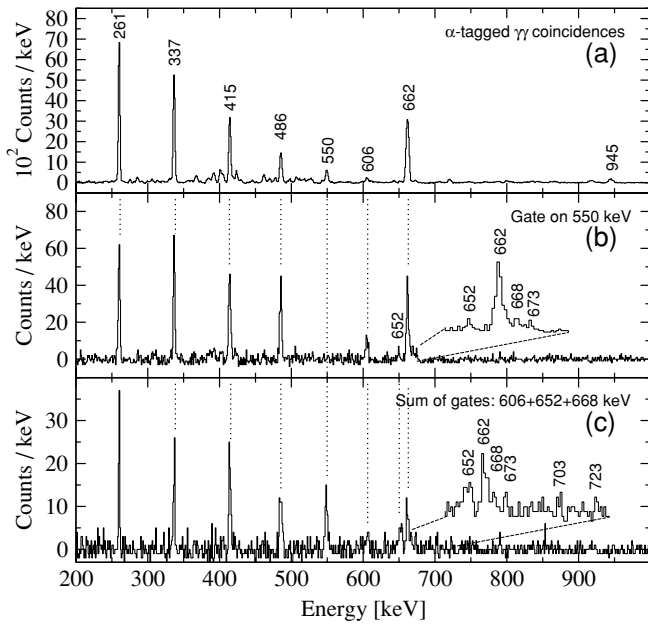


FIG. 2. Background-subtracted  $\gamma\gamma$ -coincidence  $\gamma$ -ray energy spectra (a) gated by fusion-evaporation residues and tagged with  $^{186}\text{Pb}$   $\alpha$  decays, (b) gated by the 550 keV transition, and (c) sum of gates on the 606, 652, and 668 keV transitions. Insets in (b) and (c) show magnification of the energy range around 662 keV.

On the basis of intensity limits, these transitions may still have  $B(E2)$  values of 5, 25, and 30 times higher ( $\Delta I = 0$   $M1$  transitions between  $K = 0$  bands are forbidden), respectively, than that for the  $2_2^+ \rightarrow 0_1^+$  transition (Sec. IV B). An  $I = 3$  assignment for the state at 945 keV would enhance the

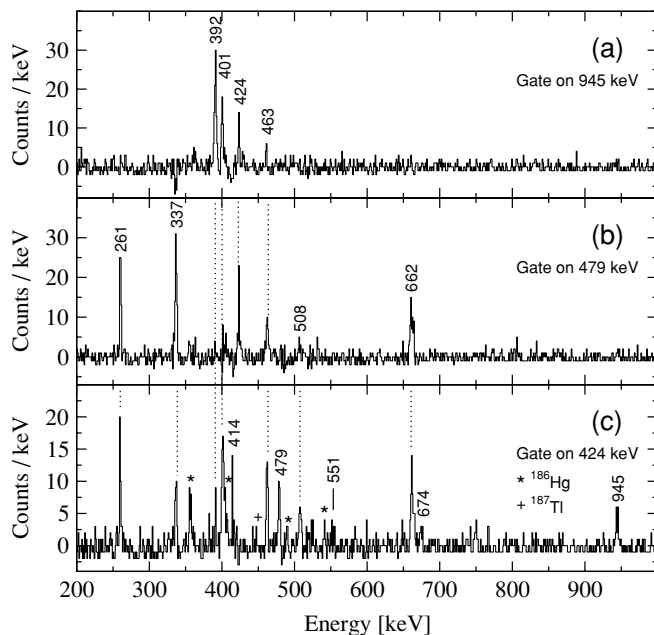


FIG. 3. Recoil-gated  $\alpha$ -tagged  $\gamma\gamma$ -coincidence spectra with gates on the (a) 945, (b) 479, and (c) 424 keV transitions. Contaminant transitions from  $^{186}\text{Hg}$  and  $^{188}\text{Tl}$  in the lowest spectrum have been marked.

$3_1 \rightarrow 2_1^+$  transition of 283 keV, and the 945 keV transition would not be observed.

The 1337 keV level is tentatively assigned as  $I^\pi = 4_2^+$  as it deexcites to the  $2_1^+$ ,  $4_1^+$ , and  $2_2^+$  states. An  $I = 3$  assignment is unlikely, as that would make the level highly non-yrast. Further support for this assignment comes from the deexcitation of the states lying above.

For similar reasons, the 1738 keV level is tentatively assigned as  $I^\pi = 6_2^+$ . The assignment is consistent with the angular distribution information for the interband 479 keV transition allowing a non-stretched  $E2$  character. Figure 3(b) shows a spectrum gated by this transition. It clearly shows the yrast-band transitions lying below, together with the transitions associated with band II lying above, the gating transition in the level scheme. This transition plays a key role in the spin assignment as it provides strong evidence for assigning the 1738 keV level with  $I^\pi = 6_2^+$ .

In addition to the  $\gamma\gamma$ -coincidence relations and intensities, the  $8_2^+$  assignment of the 2163 keV level is supported by the angular distribution information for the 424 keV transition. The spectrum in Fig. 3(c) gated by this transition shows transitions of band II up to  $I^\pi = 14^+$ . Interband and yrast-band transitions are also present.

Based on the  $\gamma\gamma$ -coincidence relations and intensity balance arguments, the 463, 508, and 551 keV transitions are assumed to form an  $E2$  cascade feeding the  $8_2^+$  state; and thus, together with the 392, 401, and 424 keV transitions, they form a  $K = 0$  band of  $E2$  transitions built on a low-lying  $0^+$  state (Sec. IV B).

It should be noted that the yrast-band transitions had an isotropic  $\gamma$ -ray angular distribution up to  $I^\pi = 8^+$ , whereas for band II and interband transitions, anisotropy was observed above the  $6_1^+$  and  $4_2^+$  levels. This is at least partly due to the overlapping  $8_1^+ \rightarrow 6_1^+$  and  $4_2^+ \rightarrow 4_1^+$  transitions, the latter resulting in a negative angular distribution coefficient.

### C. Band III

The 2593 keV level deexcites mainly via the 918 keV transition. The  $\gamma$ -ray energy spectrum gated by this transition is shown in Fig. 4(a), revealing the yrast-band transitions below the  $8_1^+$  state. In addition, the 369 and 420 keV transitions can be seen in coincidence. The 918 keV transition was placed into the level scheme as an interband transition connecting band III with the yrast band. The initial 2593 keV level is tentatively assigned with  $I^\pi = 9^\pm$  according to angular distribution information for the 918 keV transition. The angular distribution also allows an  $I^\pi = 8^+$  assignment, but that would be unlikely due to the non-observation of the  $E2(8^+ \rightarrow 6_1^+)$  transition, which would be the dominant branch because of the energy phase space factor. Further support for the level structure can be obtained from the coincidence relations shown in Figs. 4(b) and 4(c). Based on the energy sum arguments, the 306 keV transition was associated with band III.

Since the 369 keV transition overlaps with the  $2_1^+ \rightarrow 0_1^+$  transition in  $^{184}\text{Hg}$ , the structure of band III is illustrated with a spectrum gated by the 801 keV interband transition [Fig. 4(b)]. It presents the yrast-band transitions up to  $I^\pi = 10_1^+$  together with the 420, 461, and 498 keV transitions.

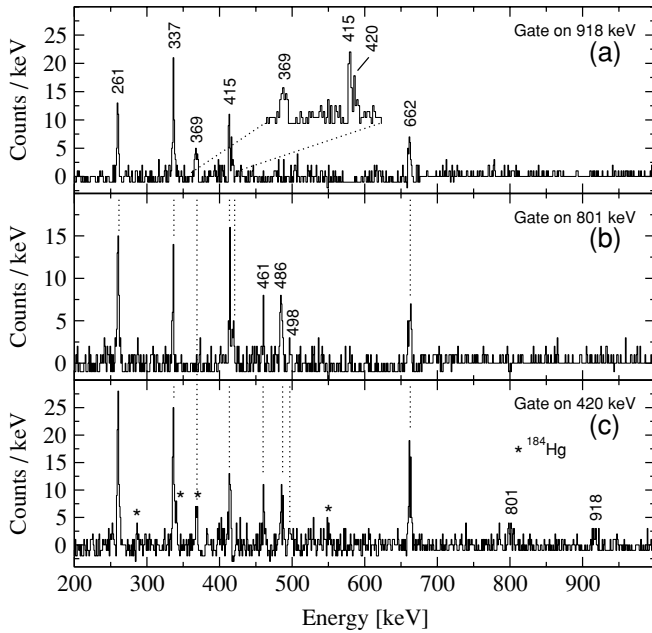


FIG. 4. Same as Fig. 3, but with gates on the (a) 918, (b) 801, and (c) 420 keV transitions. Inset of (a) magnifies the energy range 360–430 keV.

Thus, the initial state, deexcited by the 801 keV transition, lies at 2962 keV, matching with the sum of  $2593 + 369$  keV.

The third spectrum, Fig. 4(c), is gated by the 420 keV transition. This transition overlaps with the  $8_1^+ \rightarrow 6_1^+$  transition in  $^{184}\text{Hg}$ , but it was chosen because it shows all the observed transitions associated with band III. Contaminant transitions originating from  $^{184}\text{Hg}$  were easily identified. Based on their intensities, the contribution of the overlapping 368 keV  $2_1^+ \rightarrow 0_1^+$  transition of  $^{184}\text{Hg}$  in the 369 keV peak is minimal.

Based on the  $\gamma\gamma$ -coincidence relations, intensities, and angular distribution information for the  $9_1 \rightarrow 8_1^+$  transition, the 369, 420, 461, and 498 keV transitions are assumed to form an odd-spin band of  $E2$  transitions. In addition, similar bands have been observed in light Os, Pt, and Hg nuclei.

#### D. Band IV

Band IV members were placed into the level scheme on the basis of  $\gamma\gamma$ -coincidence relations and energy sum arguments. The interband transitions from this band to band I were weak, and no useful angular distribution information could be extracted for these transitions. The tentative assignments were based on intensity balance and sum energy arguments and level energy systematics of neighboring nuclei.

The energy spectra presented in Fig. 5 reveal a weak band structure at relatively low excitation energies. The uppermost spectrum is gated by the 362 keV transition, which is one of the transitions from the lowest observed state at 1307 keV. The transition feeds the  $2_2^+$  state, as the 945 keV transition is seen in coincidence. The absence of the feeding 337 keV transition is most probably due to poor statistics and difficulties in background subtraction, as its energy overlaps with that of the yrast  $6_1^+ \rightarrow 4_1^+$  transition. The gating 362 keV transition

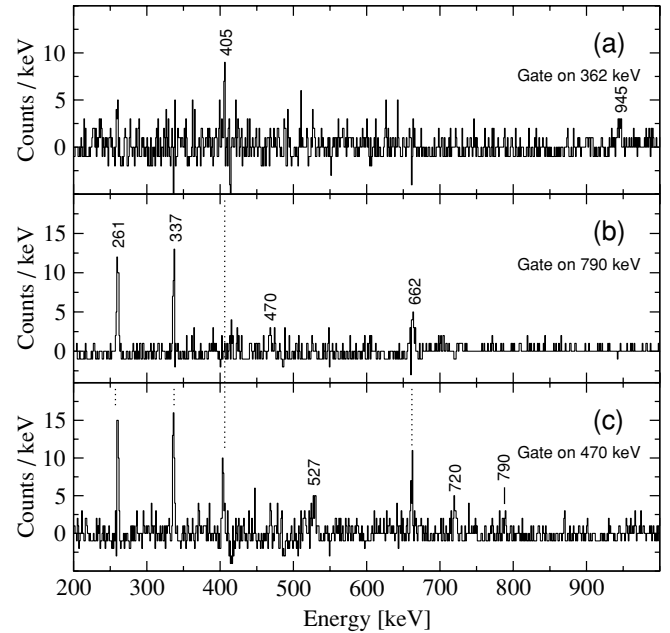


FIG. 5. Same as Fig. 3, but with gates on the (a) 362, (b) 790, and (c) 470 keV transitions.

can be seen in the spectrum shown in Fig. 3(a) (not marked) confirming coincidence with the 945 keV transition.

Figure 5(b) shows the  $\gamma$ -ray energy spectrum gated by the 790 keV interband transition assumed to feed the yrast  $6^+$  state, the initial state lying at 2049 keV. In the spectrum, the lowest yrast-band transitions are present together with the feeding 470 keV transition.

The third gate was set on the 470 keV transition, resulting in the spectrum shown in Fig. 5(c). It presents both interband and intraband transitions associated with band IV.

The construction of band IV was difficult because of several overlapping transition energies both in  $^{186}\text{Pb}$  and in  $^{186}\text{Hg}$ . The total projection of the  $\gamma\gamma$  matrix shows peaks at 645 and 384 keV (Fig. 6), which is in accordance with the energy sum balance associated with band IV. Partial support from  $\gamma\gamma$ -coincidence data encouraged association with band IV. However, because of the insufficient statistics, only tentative placement in the level scheme could be made.

#### E. Other transitions

The recoil-gated  $\alpha$ -tagged  $\gamma\gamma$ -coincidence data include several transitions that could not be placed into the level scheme on account of insufficient statistics. Such transitions are labeled in Fig. 6 and listed in Table I. Figure 6 shows the recoil-gated  $\alpha$ -tagged singles  $\gamma$ -ray energy spectrum and the total projection of the recoil-gated  $\alpha$ -tagged  $\gamma\gamma$ -coincidence matrix. If these transitions were obtained from random recoil- $\alpha$  correlations, they should originate from contaminant  $^{186}\text{Hg}$ ,  $^{184}\text{Hg}$ ,  $^{187}\text{Tl}$ , or  $^{186}\text{Tl}$  nuclei produced via the most dominant reaction channels. The 384 and 645 keV transitions can be associated with the nuclei mentioned above, but they also coincide with transitions associated with  $^{186}\text{Pb}$ . The other labeled transitions have not been observed in contaminant nuclei.

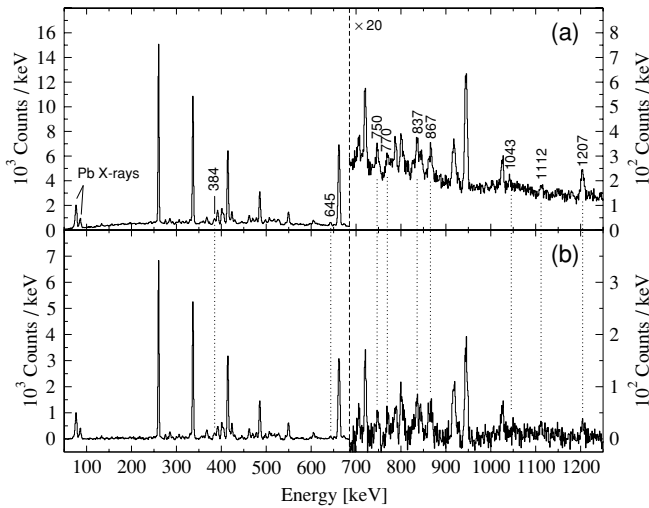


FIG. 6. Transitions that could not be placed in the level scheme together with the 384 and 645 keV transitions. (a) Recoil-gated  $^{186}\text{Pb}$   $\alpha$ -tagged singles  $\gamma$ -ray energy spectrum. (b) Total projection of the background-subtracted recoil-gated  $\alpha$ -tagged  $\gamma\gamma$  matrix.

Several prompt transitions associated with  $^{186}\text{Pb}$  are not in coincidence with the yrast-band transitions. This is partly because of insufficient statistics, but it may indicate that these transitions feed the ground state or are above an isomeric state. For example, the 1207 keV transition might be associated with a  $(1^-)$  state at 1219 keV analogous to that in  $^{188}\text{Pb}$  [40]. No clear evidence for isomeric states was observed in the present experiment.

#### IV. DISCUSSION

Figure 7 shows level energy systematics of the even-even Pb isotopes below the neutron  $N = 126$  shell closure. A systematic lowering of the first excited  $0^+$  state with decreasing neutron

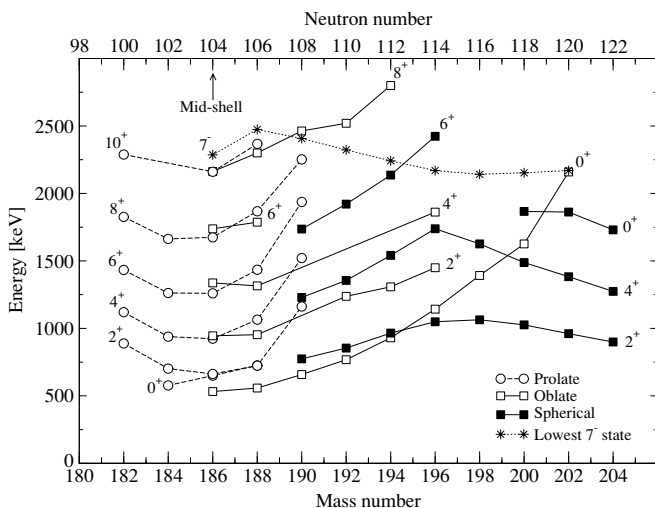


FIG. 7. Level energy systematics for even-even Pb isotopes. Data are from the present work, Refs. [5,24,40,42–52], and references therein.

number is apparent. These states are associated with a mainly oblate structure and can also be described as mainly  $\pi(2p-2h)$  shell-model intruder excitations [2,12,13,41]. In  $^{194}\text{Pb}$  and its lighter isotopes, the  $0^+$  intruder state becomes the first excited state. However,  $^{188}\text{Pb}$  is so far the only Pb isotope in which a well-developed non-yrast collective band has been observed that may well be associated with the oblate minimum [40]. The level energy systematics for candidate oblate band members in  $^{186}\text{Pb}$  and  $^{188}\text{Pb}$  follow the behavior predicted by theoretical mean-field Hartree-Fock-Bogoliubov (HFB) calculations [15,16].

#### A. Prolate yrast band

In contrast to the heavier Pb isotopes, well-developed prolate minima were predicted to occur in Pb isotopes with  $N \leq 108$  through calculations carried out in the framework of the Strutinsky shell-correction method with a Woods-Saxon potential and a monopole pairing interaction [10–12]. The first direct experimental evidence for prolate deformation in the light Pb isotopes was provided by Heese *et al.* [17]. They observed collective yrast bands in  $^{186}\text{Pb}$  and  $^{188}\text{Pb}$  by using in-beam  $\gamma$ -ray spectroscopy and associated them with a prolate shape on the basis of their similarities with rotational yrast bands in Hg isotones. Indeed, the similarities are striking, as will be described below. In-beam results for  $^{186}\text{Pb}$  were confirmed by Baxter *et al.* [18]. Later on, Andreyev *et al.* [8] determined the first two excited states in  $^{186}\text{Pb}$  to be  $0^+$  states. On the basis of  $\alpha$ -decay hindrance factors, the 532 keV  $0_2^+$  state and the 650 keV  $0_3^+$  state were associated with  $\pi(2p-2h)$  and  $\pi(4p-4h)$  configurations, respectively. In the deformation picture, these states are usually associated with an oblate and a prolate shape, respectively. The latter is assumed to be the band head of the collective yrast band. However, bands I and II are mixed to some extent, and from hereafter, a mainly prolate (oblate) band will be referred to as just a prolate (oblate) band unless otherwise stated.

The latest in-beam results for  $^{186}\text{Pb}$  (excluding the present data set) were reported by Reviol *et al.* [19]. They confirmed earlier results and proposed four new transitions (425, 464, 554, and 596 keV), two of which (554 and 596) are not supported by the present data.

In Fig. 8, the kinematic moments of inertia as a function of  $\gamma$ -ray energy are plotted for the yrast bands in the isotones  $^{182}\text{Pt}$ ,  $^{184}\text{Hg}$ , and  $^{186}\text{Pb}$  (circles) and for some of neighboring nuclei. Overall, the kinematic moment of inertia for the yrast band in  $^{186}\text{Pb}$  follows that for the corresponding band in  $^{184}\text{Hg}$  remarkably well. The curves reveal a smooth increase with increasing  $\gamma$ -ray energy (or rotational frequency) until a sudden increase at around spin  $16^+$ . This upbend in band I in  $^{186}\text{Pb}$  has tentatively been observed for the first time in the present work. In the corresponding bands in Hg and Pt nuclei, the upbend has been associated with an alignment of  $\nu(i_{13/2})^2$  or  $\pi(h_{9/2})^2$  according to cranked shell-model calculations.

The properties of these yrast bands are further considered in Fig. 9, where the aligned angular momenta  $i_x$  are plotted as a function of rotational frequency. The Harris parameters  $\mathcal{J}_0 = 27.1\hbar^2/\text{MeV}$  and  $\mathcal{J}_1 = 194.7\hbar^4/\text{MeV}^3$  used for all plots were extracted from unperturbed yrast-band states in  $^{184}\text{Hg}$ .

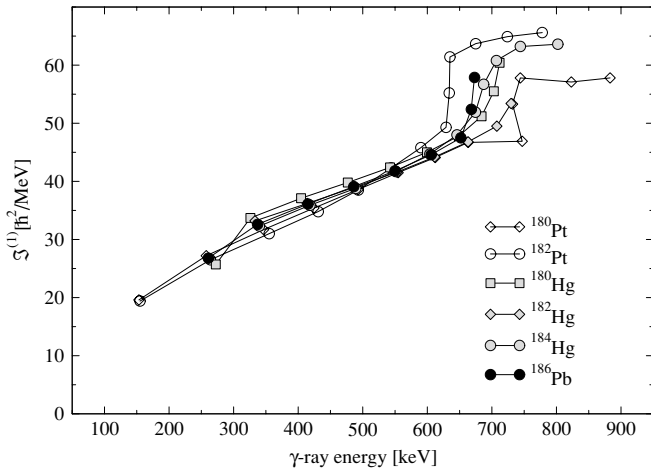


FIG. 8. Kinematic moment of inertia  $\mathcal{J}^{(1)}$  as a function of  $\gamma$ -ray energy for the collective bands in  $^{186}\text{Pb}$ ,  $^{182}\text{Pt}$ , and in  $^{180-184}\text{Hg}$ . Data for  $^{186}\text{Pb}$  are from the present work, and for other nuclei from Refs. [53–55].

The plots in Fig. 9 reveal similar alignment in  $^{186}\text{Pb}$  as in its isotones  $^{182}\text{Pt}$  and  $^{184}\text{Hg}$ . An alignment gain at crossing frequency of  $\hbar\omega \approx 0.33$  MeV for  $^{186}\text{Pb}$  can be deduced. According to theoretical quasiparticle Routhians, a proton alignment would give rise to a more drastic backbend and take place at a crossing frequency of  $\hbar\omega \approx 0.31$  MeV, whereas the alignment of a neutron pair would occur at slightly lower crossing frequency of  $\hbar\omega \approx 0.27$  MeV with higher interaction strength. The former is in better agreement with the measured crossing frequency, the latter supporting smoother neutron alignment. In lighter  $N \approx 104$  nuclei, this alignment is attributed to  $\nu(i_{13/2})^2$ . Because of these contradictions, the origin of the alignment remains unclear and has been widely discussed in various articles [18,55–57]. The data

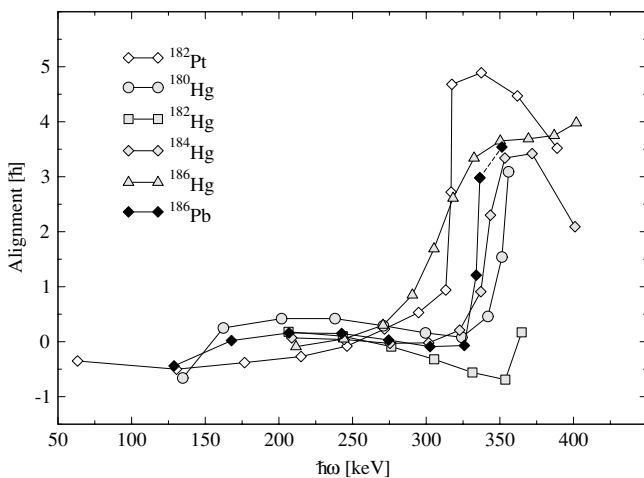


FIG. 9. Aligned angular momenta of the yrast band in  $^{186}\text{Pb}$  and of the corresponding prolate bands in Pt and Hg nuclei close to the neutron mid-shell as a function of rotational frequency. In all cases, a common reference was subtracted with Harris parameters  $\mathcal{J}_0=27.1\hbar^2/\text{MeV}$ ,  $\mathcal{J}_1=194.7\hbar^4/\text{MeV}^3$  [58]. Data for  $^{186}\text{Pb}$  are from the present work, and for other nuclei from Refs. [53,54,59–61].

also provide a hint of the  $22_1^+ \rightarrow 20_1^+$  transition with an energy of 703 keV (see Fig. 2). This transition was not placed in the level scheme, but it was used in the alignment plot (dashed line extension), thus suggesting an alignment gain of approximately  $4\hbar$ .

### B. Association of band II with oblate shape

The observation of non-yrast bands is an important step toward understanding the structure of light Pb nuclei. This section provides arguments that associate band II with an oblate shape. Further support for the association of band II with a  $2p-2h$  configuration can be found from the theoretical discussion presented in Sec. V.

Remarkable features of band II are the strong  $I \rightarrow I$  and weak  $I \rightarrow I-2$  interband transitions to the prolate yrast band, as shown in Fig. 10. The observed 674 keV branch from the  $4_2^+$  to the  $2_1^+$  state represents only about 3% of the  $B(E2)$  value of the 392 keV intraband transition. The non-observation of other  $I \rightarrow I-2$  interband transitions allows intensity limits to be set. The upper limit for their  $B(E2)$  values is determined to be lower than 3% of that of the competing intraband transitions in all cases.

If band II is a quasi- $\beta$  band based on the prolate minimum, the competing  $I \rightarrow I-2$  and  $I \rightarrow I$   $E2$  branches from band II to band I should, according to the Alaga rules [62], have similar  $B(E2)$  values. Therefore, the  $I \rightarrow I-2$  transitions having the highest energy, should be the dominant ones. This is clearly not what is observed. Similar arguments make a  $\gamma$  band an unlikely explanation for band II. A possible candidate for a  $\gamma$  band is discussed in Sec. IV D.

The observed intensities for the  $I \rightarrow I$  interband transitions from the  $4_2^+$ ,  $6_2^+$ , and  $8_2^+$  states represent  $B(E2)$  values, which

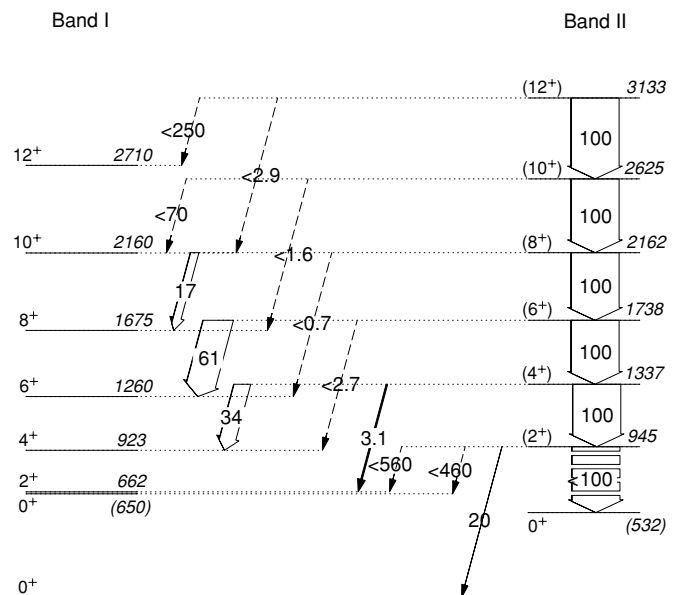


FIG. 10. Relative  $B(E2)$  values deduced for band II from the present data.  $B(E2)$  values have been normalized to 100 for the corresponding intraband transition. Arrow widths are related to the  $B(E2)$  values; transitions with deduced  $B(E2)$  upper limits are shown with dashed arrows.

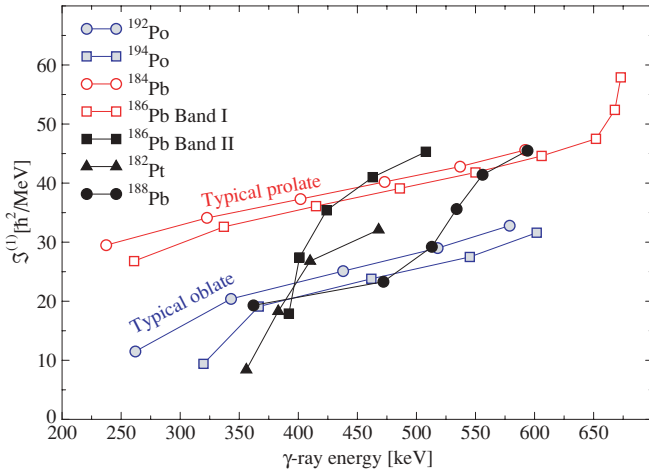


FIG. 11. (Color online) Kinematic moment of inertia  $\mathcal{J}^{(1)}$  as a function of  $\gamma$ -ray energy for bands I and II together with those for known oblate bands in nuclei close to  $^{186}\text{Pb}$ . Data for  $^{186}\text{Pb}$  are from the present work, and for the other nuclei from Refs. [40,59,63,64].

are 20–60% of those of the competing intraband transitions. The deduced intensity limits for the similar  $I \rightarrow I$  transitions from the higher lying states of band II do not rule out the existence of  $E2$  transitions of a similar strength. As pointed out by Dracoulis *et al.* [39], the strong  $I \rightarrow I$  interband transitions may be due to mixing of two different shapes.

The kinematic moments of inertia  $\mathcal{J}^{(1)}$  for band II in  $^{186}\text{Pb}$ , together with oblate bands in  $^{182}\text{Pt}$ ,  $^{188}\text{Pb}$ ,  $^{192,194}\text{Po}$ , and  $^{196}\text{Pb}$ , are plotted in Fig. 11. For comparison, the values of  $\mathcal{J}^{(1)}$  for the prolate bands in  $^{184,186}\text{Pb}$  are also shown (open symbols). In general, the kinematic moment of inertia values for the prolate bands are higher than those for corresponding oblate bands. The  $\mathcal{J}^{(1)}$  values for the  $^{192,194}\text{Po}$  nuclei plotted as representatives of well-behaving oblate rotational bands (blue/grey symbols) are lower than those for the prolate bands, but they still increase smoothly with increasing rotational frequency ( $\gamma$ -ray energy). The  $\mathcal{J}^{(1)}$  curve for band II in  $^{186}\text{Pb}$  differs from both the known prolate and the oblate bands in  $^{192,194}\text{Po}$ . Similarities in the kinematic moments of inertia plots can be found between the candidate oblate bands in  $^{182}\text{Pt}$ ,  $^{186}\text{Pb}$ , and  $^{188}\text{Pb}$  (black symbols). They extend from small  $\mathcal{J}^{(1)}$  values at low spin to values that are higher than those for the well-behaving oblate bands or even higher than those for the prolate bands, as shown in Fig. 11. It is difficult to associate these upbands with any alignment of valence nucleons, as they occur at such low spin (see, for example, Sec. IV A and references therein). One explanation would be a shape change toward a more deformed oblate structure. Highly deformed oblate structures are predicted to occur at relatively low excitation energy in the even-even Pb isotopes close to the neutron mid-shell [12,15,16].

Similar bands in even-even Pt isotopes close to  $N = 104$  have been interpreted as quasi- $\beta$  bands [56,65,66]. Those bands were associated with collective vibrations on the basis of strong  $E0$  admixtures in  $I \rightarrow I$  transitions, which is a possible signature of  $\beta$ -vibrational states. De Voigt *et al.* [56] associated the band in  $^{180}\text{Pt}$  with a quasi- $\beta$  band even though the branching ratios were in disagreement with the Alaga rules.

However, a large  $E0$  strength can be a result of mixing of states with different shapes, and by that means it can also be a sign of different deformation [67]. Such a study was recently carried out by Dracoulis *et al.* [39], where the dominant  $E0$  components in several interband  $I \rightarrow I$  transitions in  $^{188}\text{Pb}$  were reported. This argument was also used by Popescu *et al.* [59] and Hebbinghaus *et al.* [68] as they both associated the bands above the  $0_2^+$  state in  $^{182}\text{Pt}$  and in  $^{186}\text{Pt}$ , respectively, with an oblate shape.

The present coincidence data for  $^{186}\text{Pb}$  do not indicate strong  $E0$  components in the corresponding interband transitions within the statistical error bars. However, it should be noted that because of the higher energies of these transitions in  $^{186}\text{Pb}$  (414.5, 478.8, and 487.4 keV) compared to those in  $^{188}\text{Pb}$  (250.8, 352.6, and 431.7 keV, respectively), possible  $E0$  components of similar monopole strength to those in  $^{188}\text{Pb}$  may well be obscured by the much faster  $E2$  components in  $^{186}\text{Pb}$ . The  $E0$  transition rate increases very slowly with increasing transition energy [69], whereas the  $E2$  transition rate is proportional to the fifth power of the transition energy. For example, assuming the same monopole strength for both  $^{188}\text{Pb}$  and  $^{186}\text{Pb}$ , it can be deduced that the  $E0$  branch for the  $6_2^+ \rightarrow 6_1^+$  transition is roughly 10% faster in  $^{186}\text{Pb}$  than in  $^{188}\text{Pb}$ , whereas the competing  $E2$  transition is  $(479 \text{ keV}/353 \text{ keV})^5 = 4.6$  times more probable. When combined, the gain in the  $I(E0)/I(E2)$  ratio in  $^{186}\text{Pb}$  is still four times smaller than in  $^{188}\text{Pb}$  because of the higher transition energy in  $^{186}\text{Pb}$ .

### C. Candidate for an octupole band

As discussed in Sec. III C, firm spin assignments of the band III members could not be made. Nevertheless, in the following it is assumed that the 2287 keV state is the band head of band III and is assigned as  $I^\pi = (7^-)$ . The possible origin of this band is discussed below.

Negative-parity bands have been observed in several even-even Os, Pt, and Hg isotopes in the vicinity of the neutron mid-shell. However, there is no consensus regarding their origin. It has been proposed that these structures in  $^{176-180}\text{Os}$ ,  $^{176-180}\text{Pt}$ , and in  $^{178-180}\text{Hg}$  are built on a single-phonon octupole vibration, crossed by two-quasiparticle excitations at higher frequencies [53,56,70–72]. In contrast, pure two-quasiparticle assignments for low-lying negative-parity structures in  $^{184}\text{Hg}$ ,  $^{182}\text{Pt}$ , and  $^{180}\text{Os}$  have also been proposed [59,60,73]. The intrinsic structures of negative-parity bands in  $^{182}\text{Hg}$  and  $^{186}\text{Hg}$  remain unclear. Because of its similarity to these bands in the light Os, Pt, and Hg isotopes, band III is tentatively associated with negative parity.

The aligned angular momenta for bands I and III, together with yrast and  $5^-$  bands in  $^{182}\text{Pt}$ , are plotted as a function of rotational frequency in Fig. 12. The aligned angular momentum values start from approximately  $3\hbar$ , which is typical for octupole bands.  $^{182}\text{Pt}$  is chosen as a reference nucleus since it is an isotone of  $^{186}\text{Pb}$ , rather well studied, and a good representative of nuclei with corresponding negative-parity bands in this region.

The similar underlying structure of band III to the  $5^-$  band in  $^{182}\text{Pt}$  is further supported by a similar decay pattern above

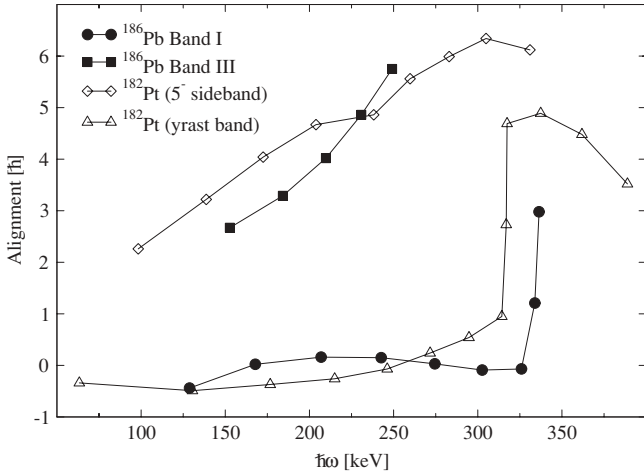


FIG. 12. Aligned angular momenta as a function of rotational frequency for bands I and III together with corresponding bands in  $^{182}\text{Pt}$ . Data for  $^{182}\text{Pt}$  are from Ref. [59].

the  $7^-$  state, although feeding of the oblate  $6^+$  state was not observed in  $^{186}\text{Pb}$ .

Band III could be considered as a candidate for an octupole band using the same arguments as put forward by Kondev *et al.* [53], though Popescu *et al.* [59] proposed the two-quasineutron scenario for the  $5^-$  band in  $^{182}\text{Pt}$ . Kondev *et al.* deduced from the level energy systematics of even-even Os, Pt, and Hg nuclei with  $N = 98-106$  that the level energies of the negative-parity bands relative to the prolate  $6^+$  state were insensitive to the neutron number. Thus, being based on the prolate minimum, this deduction contradicts the two-quasineutron scenario. The same phenomenon is observed in Pb isotopes, as the energy of the candidate  $7^-$  state in  $^{186}\text{Pb}$  deviates from the smooth systematic behavior of  $7^-$  states in heavier Pb isotopes and follows the behavior of the prolate states, as seen in Fig. 7.

#### D. Low-lying odd-spin band

Low-lying  $\gamma$  vibrations are expected to evolve in nuclei having broad and shallow minima in their potential energy surfaces. Such circumstances are common, for example, in semimagic nuclei close to the mid-shell. The present work obtained support for the association of band IV with  $\gamma$  vibration. The interband transitions between the even-spin and odd-spin states in  $\gamma$  bands are rarely observed; therefore, it is relevant to consider only even-spin or odd-spin sequences of the  $\gamma$  band. Little evidence for low-lying odd-spin bands has been observed in the Pb isotopes, except recently in  $^{188}\text{Pb}$  [40]. A few low-lying bands in light Pt isotopes associated with  $\gamma$ -vibrational structures [56,59,68] resemble the band IV observed in the present work. The possibility that band II consists of the even-spin states of a  $\gamma$ -vibrational band rather than oblate states cannot be fully excluded. However, this would be against the arguments supporting the oblate intrinsic structure of band II given in Sec. IV B. It is also difficult to associate band IV with any two-quasiparticle excitation, as it lies relatively low in energy.

In Fig. 13, the bands related to band IV have been compared with the corresponding bands in the isobar  $^{186}\text{Pt}$ . The level

schemes are normalized to the energy of the  $6_1^+$  states. There are deviations in the corresponding intraband transition energies, but the decay patterns of the odd-spin states of the candidate  $\gamma$  bands are fairly similar. The even-spin states of the  $\gamma$  band in  $^{186}\text{Pt}$  are also shown to illustrate the clustering of the  $\gamma$ -band levels. Those states deexcite via  $I \rightarrow I$  and  $I \rightarrow I - 2$  transitions to the prolate yrast band (not shown in Fig. 13), but no linking transitions to the odd-spin states have been observed. Applying the even-spin states of the  $\gamma$  band in  $^{186}\text{Pt}$  to  $^{186}\text{Pb}$ , the clustering of  $\gamma$ -band levels as  $(3^+, 4^+), (5^+, 6^+), \dots$  is evident. Such staggering is a signature of  $\gamma$  softness and is typical of  $\gamma$  bands observed in light Pt isotopes. This is peculiar to nuclei exhibiting broad and shallow minima in nuclear potential energy surfaces, as is the case in  $^{186}\text{Pb}$  [8,15]. It can also be seen that the even-spin states of the  $\gamma$  band would be almost degenerate with the states of band II, thus resulting in mixing with the  $K = 0$  band. In the presence of mixing, the even-spin states would be pushed up in energy, whereas the odd-spin states remain unperturbed because of the absence of other positive-parity odd-spin states. Such mixing would introduce  $K = 2$  admixture into the  $K = 0$  bands, enabling  $M1$  components in the  $I \rightarrow I$  transitions. This possibility has been discussed by Dracoulis *et al.* [40] for  $^{188}\text{Pb}$ , where the candidate for the odd-spin sequence of the  $\gamma$  band was observed. Feeding of the oblate band from the candidate  $\gamma$  band is also observed in  $^{186}\text{Pb}$ , whereas the corresponding interband transitions remain unobserved in even-even isotopes  $^{182-186}\text{Pt}$ . This fact would support the interpretation that the oblate states and the even-spin states of the  $\gamma$  band are mixed in  $^{186,188}\text{Pb}$  to some extent. However, transitions from the  $K = 0$  bands to  $\gamma$  bands have been observed in Pt nuclei, suggesting mixing between the bands. Mixing would also explain the non-observation of the even-spin candidates of the possible  $\gamma$  band as the states would be highly non-yrast.

The deduced branching ratios of the odd-spin states of the  $\gamma$  band relative to corresponding intraband transition are listed in Table II. The upper limits for the  $B(E2)$  values of the non-observed transitions were set by estimating the number of counts needed in order to produce a peak at the expected  $\gamma$ -ray energy in a spectrum gated by the feeding transition.

TABLE II. Comparison of the relative branching ratios for interband transitions in  $^{186}\text{Pb}$  (present work) and  $^{186}\text{Pt}$  [68]. The non-observation of certain transitions allowed upper limits for several  $B(E2)$  values to be set.

$I_{\text{initial}}^{\pi}$	$B(E2)$	$B(E2)$	$B(E2)$
	$I \rightarrow I - 2$ [intraband]	$I \rightarrow I - 1$ [to band I]	$I \rightarrow I - 1$ [to band II]
$^{186}\text{Pb}$			
$5_1^+$	100(30)	6(2)	<170
$7_1^+$	100(40)	5(2)	<140
$9_1^+$	100(30)	<3	<100
$^{186}\text{Pt}$			
$5_1^+$	100(40)	10(4)	–
$7_1^+$	100(7)	2.1(2)	–
$9_1^+$	100(20)	0.7(2)	–

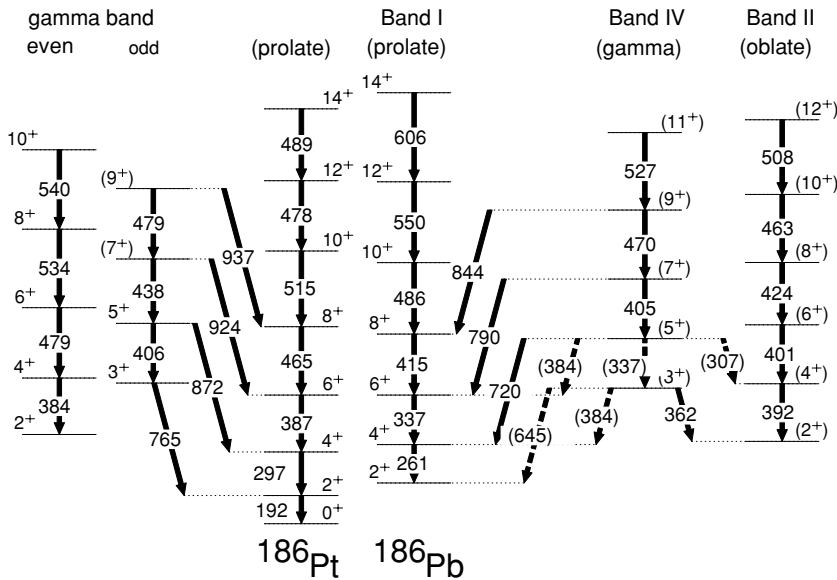


FIG. 13. Comparison between the proposed  $\gamma$ -vibrational bands in  $^{186}\text{Pb}$  and in  $^{186}\text{Pt}$  together with the prolate and oblate bands observed in these nuclei. Level schemes have been lined up with the  $6_1^+$  levels. Data for  $^{186}\text{Pt}$  are from Ref. [68].

Unfortunately, weak population of levels with spins less than 5 and impure gating conditions prevented deduction of these ratios for the decay of the  $3^+$  state. However, the available branching ratios are in accord with the corresponding ones in  $^{186}\text{Pt}$ . They also fulfill the rule of thumb that the interband transitions are approximately an order of magnitude slower than the intraband transitions.

### E. Isomeric states in $^{186}\text{Pb}$

Isomeric states have been observed in several even-even nuclei in the vicinity of  $^{186}\text{Pb}$  (see, for example, [24,40,74,75] and references therein). The level energy systematics for even-even Pb isotopes reveals a parabolic behavior of the level energies of the  $I^\pi = 11^-$  and  $I^\pi = 12^+$  isomers with a minimum at  $N = 108$ . This behavior has been reproduced by a Skyrme-Hartree-Fock-Bogoliubov calculation for the  $11^-$  isomer in Pb and Po isotopes [76], which predicted the isomer to be a few hundred keV higher for  $N = 104$  than for 106. The  $11^-$  and  $12^+$  isomers have been associated with the oblate  $\pi [(h_{9/2}[505]9/2^-) \otimes (i_{13/2}[606]13/2^+)]$  and spherical  $\nu(i_{13/2})^{-2}$  configurations in  $^{188}\text{Pb}$  with lifetimes of 38 and 136 ns, respectively [40]. When extrapolated to  $^{186}\text{Pb}$ , an increase in the excitation energy relative to the prolate  $I^\pi = 10_1^+$  state is obvious (see Fig. 7). Thus, the lifetimes of those states deexciting to the  $I^\pi = 10_1^+$  state would be much shorter, enabling a prompt observation at the target location.

No evidence for isomeric states was observed in the present work. However, the existence of isomeric states in  $^{186}\text{Pb}$  is certainly not excluded by the present results, as the transmission time through RITU (500 ns) is considerably longer than the expected lifetimes. Thus, the possible isomeric states would most likely decay in flight, never reaching the focal-plane detection system with the current reaction.

An  $8^-$  isomeric state with a lifetime of 1.2  $\mu\text{s}$ , corresponding to the Nilsson configuration  $\nu[(i_{13/2}[624]9/2^+) \otimes (f_{7/2}[514]7/2^-)]$ , has been found in  $^{188}\text{Pb}$  and associated with a prolate shape [77]. If this state was present

in  $^{186}\text{Pb}$ , it would lie at approximately 2600 keV, i.e., close to the  $9^-$  state. Excluding the 306 keV transition, band III could be considered to be built on an  $8^-$  state. It is intriguing to consider whether this state could be associated with the isomeric  $8^-$  state in  $^{188}\text{Pb}$ . However, the decay pattern of band III does not correspond to the one based on the  $8^-$  isomer in  $^{188}\text{Pb}$ . Especially, the strong intraband  $M1$  transitions above the  $8^-$  state in  $^{188}\text{Pb}$  are clearly not what is observed in  $^{186}\text{Pb}$ . Moreover, the  $8^-$  isomeric state in  $^{186}\text{Pb}$  would have a lifetime too long to be detected as prompt coincidence, even if the gain in the transition strength due to the energy factor was taken into account.

## V. THEORETICAL DESCRIPTION OF THE NEUTRON-DEFICIENT LEAD NUCLEI

The very long series of even-even Pb nuclei, starting from the region of nuclei near stability and moving into the very neutron-deficient mass region near the  $N = 104$  neutron mid-shell, forms a unique series of isotopes in which the interplay between shell-model degrees of freedom and collective modes of motion can be studied in great detail (see Fig. 7). One of the most dramatic effects arises from the smooth and systematic decrease in excitation energy of an excited  $0^+$  state (which even becomes the first excited state over all spins) with increasing number of neutron valence holes in the  $N = 126$  closed neutron shell. As discussed earlier, these Pb isotopes can be described by models relying on two complementary views of the coexisting  $0^+$  states. The first description is based on mean-field approaches and relies on the coexistence of energy minima of different shapes. The second is based on the shell model, with a description of the different states by specific  $np$ - $nh$  excitations. In the next sections, detailed theoretical analyses of  $^{186}\text{Pb}$  based on both models are presented.

Both models can serve as a starting point to go beyond a description in terms of a pure configuration, identified either by

its shape or by its  $np$ - $nh$  structure. Deformed mean-field states can be mixed in the framework of the generator coordinate method (GCM), as shell-model configurations are mixed in the interacting shell model. A nice feature of both generalized models is that it is still possible to analyze complicated states in terms of more intuitive configurations and, thanks to that, label the states as mainly oblate or 2p-2h configurations. In the same way, the theoretical bands which will be presented are not constructed by taking their intrinsic structure as a criterion. Instead, the calculated  $B(E2)$  values are used to define the bands such that the intraband  $B(E2)$  values dominate the interband  $B(E2)$  values. This is done because the percentage of mixing changes along these collective bands and, in the lower part of the bands, considerable mixing no longer allows a simple interpretation in terms of (almost) pure bands.

### A. Mean-field calculations

The specific lowering in excitation energies in Pb isotopes hints at the onset of deformed intrinsic structures that can be analyzed using a deformed mean-field approach. Calculations using either phenomenological deformed potentials (Nilsson, Woods-Saxon) [10–12] or, more microscopically, a Hartree-Fock+BCS approach [13–16] have been carried out over the years. In both kinds of calculations, the spherical ground state coexists with a low-lying oblate structure below  $A = 194$ . A prolate minimum which appears as a shoulder in the deformation energy curve of  $^{194}\text{Pb}$  develops into a minimum when the neutron number decreases further, and it becomes the first excited state in the mid-shell isotopes.

It was recognized very early [10–13] that a mean-field description is not truly valid when the potential energy surface of a nucleus presents coexisting minima, spherical and deformed, which are close in energy and not separated by a large barrier, as is the case for the neutron-deficient Pb isotopes. In such a case, it is necessary to perform a configuration-mixing calculation to obtain a reliable result. Starting from a mean-field calculation, the deficiencies of this description are corrected step by step. First, a set of HFB or HF+BCS wave functions is generated as a function of a collective variable, usually the axial quadrupole moment, using an effective nucleon-nucleon interaction. These wave functions are then projected in order to restore two of the symmetries broken at the mean-field level: particle number and angular momentum. The angular-momentum projection decomposes the mean-field states into the full spectrum of possible values of  $J$ . For each value of  $J$ , the projected wave functions are then mixed with respect to the quadrupole moment. The weights of the mixing are determined by a variational minimization of the energy, which is equivalent to the diagonalization of the nuclear Hamiltonian within the space spanned by the projected mean-field states. This generates several eigenstates corresponding to the lowest state and to excited states separately for each angular momentum  $J$ . The same effective interaction is used to generate the mean-field states and for the shape mixing.

A few comments are in order to correctly situate this approach with respect to pure mean-field calculations and to

the shell model. The final result of a configuration mixing is a full spectrum corresponding to the collective mode used to generate the deformation energy curve. The projection on angular momentum is equivalent to a transformation from the intrinsic frame of reference of the nucleus to the laboratory system. In contrast to pure mean-field methods, this approach can calculate transition probabilities between any states directly from the electromagnetic operators without relying on approximations. The resulting states can be grouped into bands according to their transition probabilities. Since the starting point of the method is a set of mean-field wave functions, one can always determine the dominant components of a state in the laboratory system of reference and label it as (predominantly) oblate, spherical, or prolate, although these labels have a meaning only in the intrinsic frame of the nucleus. There are no free parameters in such a method; the calculation relies only on an effective interaction (the SLy6 parametrization of the Skyrme force in the present study) which has been adjusted on very general nuclear properties. Inevitably, the lack of possibility to fine tune the results may lead to discrepancies with the experimental data. However, this will also allow the discrepancies to be directly related to the basic properties of the effective interactions.

A limitation of this model is that the symmetries of the building blocks, the mean-field wave functions, limit the kinds of states that can be described. Since the only constraint that has been used is the axial quadrupole moment, the effects of both triaxiality and octupole deformation are excluded. Deformation enables a large number of two-quasiparticle excitations to be generated in an economic manner, while they have to be introduced explicitly in a shell-model treatment. However, time reversal invariance is imposed at the mean-field level, which excludes any two-quasiparticle excitations in which the quasiparticles are not paired by time reversal invariance.

Systematic calculations of the neutron-deficient Pb isotopes using either a Skyrme [15] or a Gogny [16] interaction have been published recently. Results obtained in both cases are qualitatively similar, which gives good confidence in the reliability of the effective interactions. In  $^{186,188}\text{Pb}$ , nearly degenerate oblate and prolate minima in the quadrupole energy surface coexist with the spherical ground state. After symmetry restoration and configuration mixing, the ground state remains dominated by near-spherical configurations, while two bands, one predominantly prolate and the other predominantly oblate, appear at low excitation energies. In the following, some new results for  $^{186}\text{Pb}$ , obtained under the same conditions as in Ref. [15], will be presented.

The wave functions obtained from configuration mixing permit collective wave functions to be defined (see Fig. 3 of Ref. [14]). For the  $0^+$  ground state, one obtains a wide spreading around the spherical mean-field configuration. This is a typical result for the ground states of nuclei that can be classified as (anharmonic) spherical vibrators. By contrast, the first and second excited  $0^+$  states are dominated by either prolate and oblate configurations, respectively. Looking at the  $2^+$  and  $4^+$  collective wave functions, one can see that they are even more dominated by only one kind of deformation, either prolate or oblate.

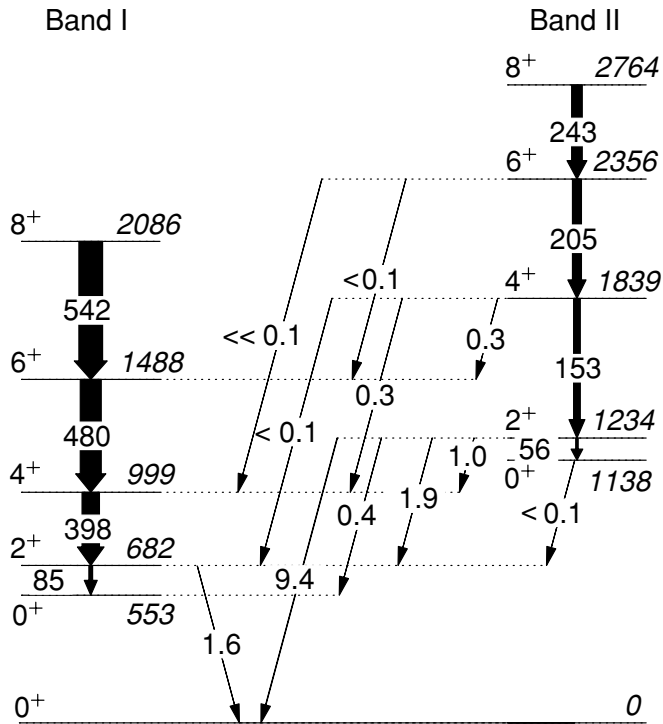


FIG. 14. Partial level scheme of  $^{186}\text{Pb}$  obtained by configuration mixing.  $B(E2)$  values shown between all the states are given in Weisskopf units.

This topography is reflected in the  $E2$ -transition probabilities presented in Fig. 14. The intraband transitions dominate, particularly when the spin increases, and are larger in the predominantly prolate band (band I). At the bottom of band II, there are rather large interband transition probabilities. In particular, the transition probabilities from the  $2_2^+$  state to the ground state and the  $2_1^+$  states are rather large.

Comparing these results with the experimental data of Fig. 10, one sees that the excitation energy of the theoretical “prolate” band is close to the experimental value, while the oblate band is slightly too high. The bands are too spread in energy (the moments of inertia are too low), which is a known deficiency of this kind of approach and is probably related to a problem of configuration space. The deexcitation probabilities of the oblate  $2^+$  state to the ground and to the oblate  $0^+$  states agree well with the experimental data, but the deexcitation to prolate  $0^+$  and  $2^+$  are underestimated; this seems to point out that the configuration mixing in the collective wave functions is not large enough, making the prolate and oblate configurations too much confined. The interband transitions with  $I \rightarrow I$  are significantly faster than those with  $I \rightarrow I - 2$ , also in agreement with the experimental data. Finally, the  $B(E2)$  values for band I agree well with the recently measured lifetimes of yrast states in  $^{186}\text{Pb}$  [78].

To analyze the structure of the bands in more detail, one can define intrinsic quadrupole moments from both the intraband transition probabilities (giving an intrinsic transition quadrupole moment  $Q^t$ ) and the spectroscopic quadrupole moments (giving an intrinsic spectroscopic moment  $Q^s$ ). The

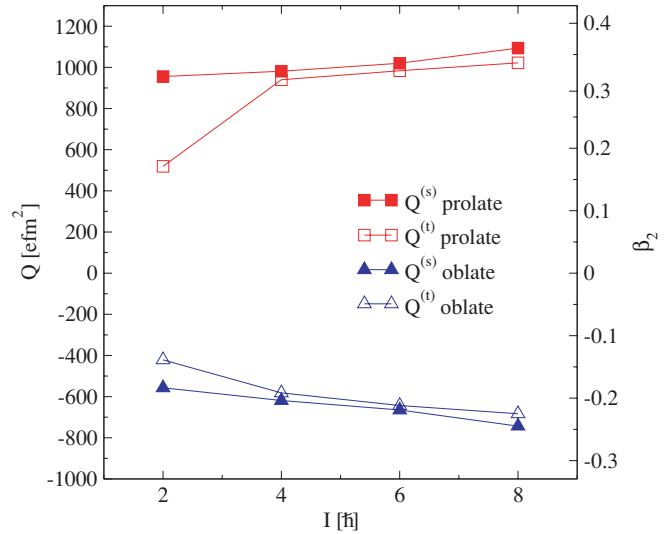


FIG. 15. (Color online) Intrinsic quadrupole moments derived from the transition and spectroscopic moments in  $^{186}\text{Pb}$  obtained by configuration mixing.

formulas that have to be used to define these moments are given in Ref. [15] (and references therein). These intrinsic moments are plotted in Fig. 15. The negative signs obtained for band II confirm that it is predominantly oblate. Close values for both moments mean that the states can be safely identified with either an oblate or a prolate shape, which is the case for all states except for the  $2_1^+$ . However, these moments vary with spin, indicating that the configuration mixing varies with  $J$  within each band.

### B. Truncated shell-model approach: The interacting boson model approximation

Over the years, experimental hints for proton pair excitations across the  $Z = 82$  closed proton shell have accumulated, in particular through the study of  $\alpha$ -decay hindrances [8]. Although the unperturbed energy of these  $np$ - $nh$  excitations is initially very high thanks to the large proton shell gap, the pairing and the strong quadrupole interaction between protons and neutrons causes the characteristic lowering of these excitations to very low energy near neutron mid-shell [79,80]. Unfortunately, large-scale shell-model approaches that can take into account both the full active neutron shell (between  $N = 82$  and  $N = 126$ ) and the  $np$ - $nh$  excitations across the  $Z = 82$  proton shell are totally out of computational reach. Consequently, one needs a truncation in which the proton  $np$ - $nh$  excitations can be included and which preserves the pairing and quadrupole proton-neutron ( $p$ - $n$ ) components of the interaction. Such a truncation is provided by the interacting boson model (IBM), which approximates nucleon pairs as  $s$  ( $L = 0$ ) and  $d$  ( $L = 2$ ) bosons, thus reducing the model space tremendously. When, in extension, the intruder nucleon pairs are also treated as genuine  $s$  and  $d$  bosons, it turns out that the multiparticle-multihole model space becomes tractable within the configuration-mixed IBM. The early formulation by Barrett and Duval [81] has been refined and reformulated to

study the Pb nuclei [82,83]. Although mean-field calculations suggest the presence of more complex excitations in the Pb isotopes, the IBM calculation is in first approximation restricted to the dominant 2p-2h and 4p-4h excitations. For this calculation, a symmetry, albeit broken, related to the active number of proton pairs was used. When comparing the yrast band in the Pb nuclei (for  $A = 184, 186, 188$ ) with the ground-state band in the W nuclei and the intruder (or prolate) band in the Pt nuclei, both for the same number of neutrons and normalizing to the  $8^+$  states, almost identical bands appear. This is connected to a symmetry similar to isospin which transforms particle proton pairs into hole proton pairs when moving through a given intruder spin multiplet (in the case of Pb,  $I = 2$ ) [84].

In the configuration-mixed IBM, the Hamiltonian for three-configuration mixing can be written as

$$\hat{H} = \hat{H}_{\text{reg}} + \hat{H}_{2\text{p-2h}} + \hat{H}_{4\text{p-4h}} + \hat{V}_{\text{mix},1} + \hat{V}_{\text{mix},2}, \quad (1)$$

with

$$\hat{H}_{\text{reg}} = \epsilon_{\text{reg}} \hat{n}_d + \kappa_{\text{reg}} \hat{Q}_{\text{reg}} \cdot \hat{Q}_{\text{reg}}, \quad (2)$$

$$\hat{H}_i = \epsilon_i \hat{n}_d + \kappa_i \hat{Q}_i \cdot \hat{Q}_i + \Delta_i, \quad (3)$$

$$\hat{V}_{\text{mix},i} = \alpha_i (s^\dagger s^\dagger + s s) + \beta_i (d^\dagger \cdot d^\dagger + \tilde{d} \cdot \tilde{d}), \quad (4)$$

where

$$\hat{Q}_i = (s^\dagger \tilde{d} + d^\dagger \tilde{s})^{(2)} + \chi_i (d^\dagger \tilde{d})^{(2)} \quad (5)$$

is the quadrupole operator. In the Hamiltonian (1),  $\hat{H}_{\text{reg}}$  operates on the regular configuration with  $N$  bosons, while the operators  $\hat{H}_{2\text{p-2h}}$  and  $\hat{H}_{4\text{p-4h}}$  act on the intruder configurations with  $N + 2$  and  $N + 4$  bosons, respectively.  $\hat{V}_{\text{mix},1}$  describes the interaction between the  $N$  and  $N + 2$  configurations, and  $\hat{V}_{\text{mix},2}$  acts between the  $N + 2$  and  $N + 4$  configurations.

The  $E2$ -transition operator is defined as

$$\hat{T}(E2) = \sum_{i=1}^3 e_i [(s^\dagger \tilde{d} + d^\dagger \tilde{s})^{(2)} + \chi_i (d^\dagger \tilde{d})^{(2)}]. \quad (6)$$

More details on the notation and choice of parameters can be found in Refs. [82,83]. Parameters  $\epsilon$ ,  $\kappa$ , and  $\chi$  are determined in [83] on the basis of intruder spin symmetry. The energy  $\Delta_{2\text{p-2h}}$  needed to excite two particles across the closed  $Z = 82$  proton shell gap corrected with the pairing and monopole energy was obtained following the procedure described in Ref. [82]. Thanks to recently measured  $B(E2)$  values for  $^{186,188}\text{Pb}$  [78], a better estimate for the mixing parameters  $\alpha_i$  and  $\beta_i$  can be obtained. Compared to the level energies,  $B(E2)$  values are far more sensitive to the precise value of  $\alpha_i$  and  $\beta_i$ . The new measured  $B(E2)$  values allow much more refined values to be extracted. As already suggested in Ref. [82], the parameters for mixing between the 2p-2h and the 4p-4h configuration ( $\alpha_2, \beta_2$ ) were slightly overestimated, whereas the mixing parameters between the regular and the 2p-2h configuration ( $\alpha_1, \beta_1$ ) had to be increased. An overview of all the discussed parameters is presented in Table III. Except

TABLE III. Parameters of Hamiltonian (1) for  $^{186}\text{Pb}$ .  $\epsilon$ ,  $\kappa$ , and  $\chi$  were determined in Ref. [83] on the basis of intruder spin symmetry. All these parameters, except for  $\Delta$ , are taken as constants for  $^{186-196}\text{Pb}$ .

	Reg	2p-2h	4p-4h
$\epsilon$ (MeV)	0.92	0.51	0.55
$\kappa$ (MeV)	0	-0.014	-0.020
$\chi$	0	0.515	-0.68
$\alpha = \beta$ (MeV)		0.018	0.018
$\Delta$ (MeV)	0	2.129	4.258
$e$ (e b)	0.110	0.140	0.170

for  $\Delta$ , all these parameters are kept constant for  $^{186-196}\text{Pb}$ . The resulting level scheme for  $^{186}\text{Pb}$  is depicted in Fig. 16. Band I has a mainly 4p-4h structure, while band II is of predominantly 2p-2h character. The mixing amplitudes of the  $0_2^+$  and the  $0_3^+$  states are similar to the results derived by Page *et al.* [85], although the mixing is somewhat more pronounced.

In addition to bands I and II, the IBM calculation shows the existence of higher lying bands, of which the lowest odd-spin band and the lowest additional even-spin band are presented in Fig. 16. Both these bands are of predominantly 2p-2h character. Although the energies of the levels in the odd-spin band deviate from the experimental ones, the level spacings differ by an almost constant factor from the experimental spacings throughout the band. Table IV lists the  $B(E2)$  ratios for the  $I \rightarrow I - 1$  interband and the  $I \rightarrow I - 2$  intraband transitions. These ratios are consistent with the experimental ones shown in Table II and support the idea that this theoretical odd-spin band might correspond to the experimental candidate  $\gamma$  band.

Continuing with the discussion of bands I and II, it can be demonstrated that the relative signs of the parameters  $\chi_{2\text{p-2h}}$  and  $\chi_{4\text{p-4h}}$  are responsible for the characteristic structure of the interband transitions. In the language of the collective model, this implies that prolate-oblate mixing is needed to reproduce the measured relative  $B(E2)$  ratios.

In order to extract collective information from the IBM, one is required to calculate the expectation value of the Hamiltonian in a coherent state basis [86–89]. For a Hamiltonian of the type in Eq. (2), this gives rise to the following potential

TABLE IV.  $B(E2)$  values in Weisskopf units for the interband and intraband transitions starting from the odd-spin band IV calculated in the framework of IBM. Values in parentheses indicate the ratios normalized to corresponding intraband transitions.

$I_{\text{initial}}^\pi$	$B(E2)$	$B(E2)$	$B(E2)$
	$I \rightarrow I - 2$ [intraband]	$I \rightarrow I - 1$ [to band I]	$I \rightarrow I - 1$ [to band II]
$5_1^+$	126 (100)	3.12 (2.5)	8.97 (7.1)
$7_1^+$	179 (100)	2.09 (1.2)	4.46 (2.5)
$9_1^+$	201 (100)	1.24 (0.6)	2.47 (1.2)

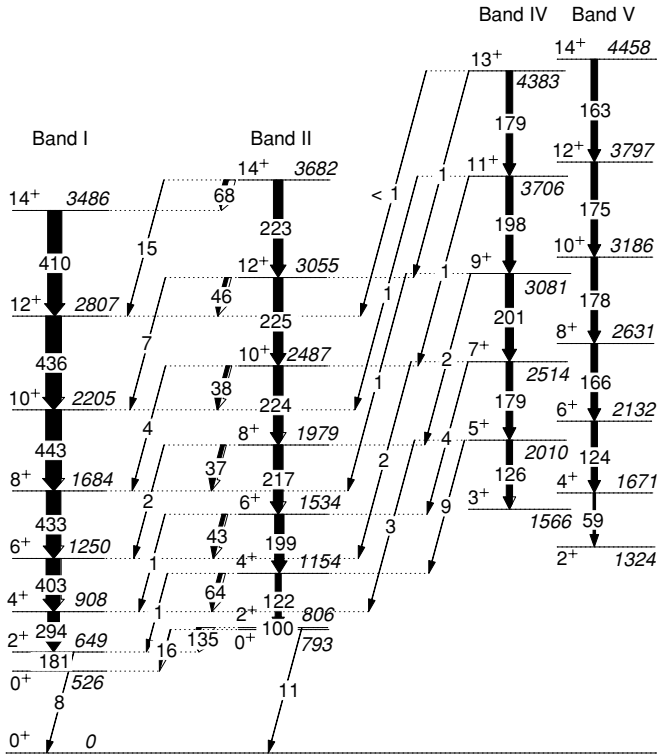


FIG. 16. Partial level scheme of  $^{186}\text{Pb}$  calculated in the framework of IBM. Instead of transition energies,  $B(E2)$  values expressed in Weisskopf units are shown.

energy surface (PES):

$$V_N = \frac{N\epsilon\beta^2}{1+\beta^2} + \kappa \left[ \frac{N(5 + (1 + \chi^2)\beta^2)}{1 + \beta^2} + \frac{N(N-1)}{(1 + \beta^2)^2} \times \left( \frac{2}{7}\chi^2\beta^2 - 4\sqrt{\frac{2}{7}}\chi\beta^3\cos(3\gamma) + 4\beta^2 \right) \right], \quad (7)$$

with  $N$  the number of bosons,  $(\beta, \gamma)$  collective variables, and  $(\epsilon, \kappa, \chi)$  the parameters occurring in the Hamiltonian of Eq. (2). Substituting the parameters of the SU(3) dynamical symmetry limit gives rise to a prolate ( $\epsilon = 0, \chi = -\sqrt{7}/2$ ) or oblate ( $\epsilon = 0, \chi = \sqrt{7}/2$ ) minimum of the PES. Similarly, it can be shown that the positive sign of  $\chi_{2p-2h}$  corresponds to an oblate deformation, and the negative sign of  $\chi_{4p-4h}$  to a prolate deformation. However, it is important to note that the level scheme resulting from these IBM calculations is rather independent of the relative signs of  $\chi_{2p-2h}$  and  $\chi_{4p-4h}$  thanks to the  $\hat{Q} \cdot \hat{Q}$  term in the Hamiltonian. The only term in the Hamiltonian sensitive to the relative sign is  $\hat{V}_{\text{mix}}$ . Hence, in the case of  $^{186}\text{Pb}$ , it is possible to alter the sign of  $\chi_{2p-2h}$ —so that the unperturbed band II is built on a prolate minimum—and to preserve a good correspondence with the experimental level scheme. The  $E2$ -transition operator [Eq. (6)], on the contrary, is very sensitive to the sign of  $\chi$ . Therefore, especially the interband  $E2$  transitions will be sensitive to changes in the relative sign of  $\chi_{2p-2h}$ . In Fig. 17, the  $B(E2)$  ratios calculated using the parameters in Table III are compared with the

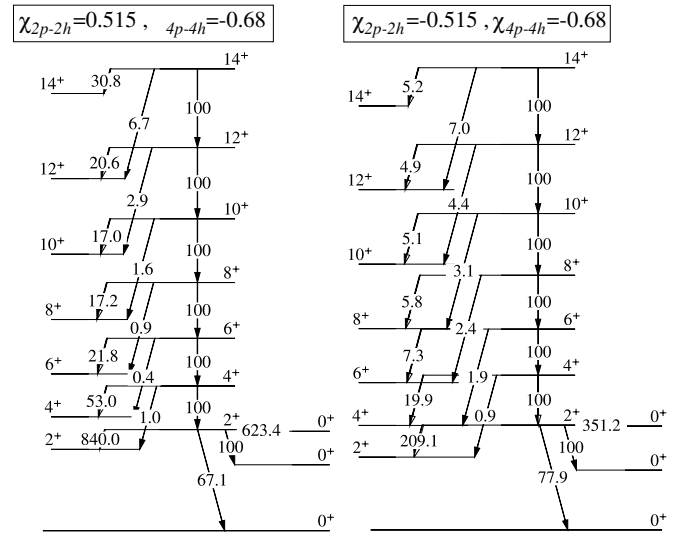


FIG. 17.  $B(E2)$  ratios in  $^{186}\text{Pb}$  calculated in the framework of IBM.

resulting ratios when both  $\chi_{2p-2h}$  and  $\chi_{4p-4h}$  are chosen to be negative, i.e., in the case of prolate-prolate mixing.

One clearly notices that although the experimental level scheme is still reproduced rather well, the  $I \rightarrow I$  and the  $I \rightarrow I - 2$  interband transitions become of the same order of magnitude when both  $\chi_{2p-2h}$  and  $\chi_{4p-4h}$  are negative. It is noteworthy that because of the inherent symmetries of the IBM, only a change in the relative signs of  $\chi_{2p-2h}$  and  $\chi_{4p-4h}$  causes the changes in the typical pattern of the  $B(E2)$  ratios. Hence, assuming that the unperturbed band I is built on a prolate minimum, it can be stated that the observed  $B(E2)$  ratios can only be described adequately when the unperturbed band II is built on an oblate minimum. The assumption that the latter band is built on a prolate minimum gives rise to approximately equally strong  $I \rightarrow I - 2$  and  $I \rightarrow I$   $E2$  transitions, which are in contradiction with the experimentally observed pattern.

Finally, it is possible to construct a PES in  $\beta$  and  $\gamma$  for the configuration mixed system following a technique explained in Ref. [90]. Summarized, the matrix coherent state approach which allows a PES to be constructed for a single configuration is applied to the IBM Hamiltonian for three-configuration mixing. Once the PES [Eq. (7)] for the three different configurations ( $N, N+2$ , and  $N+4$  bosons) are calculated, a  $3 \times 3$  potential energy matrix can be constructed as

$$\begin{pmatrix} V_N(\beta, \gamma) & \Omega_{N, N+2}(\beta) & 0 \\ \Omega_{N, N+2}(\beta) & V_{N+2}(\beta, \gamma) + \Delta_{2p-2h} & \Omega_{N+2, N+4}(\beta) \\ 0 & \Omega_{N+2, N+4}(\beta) & V_{N+4}(\beta, \gamma) + \Delta_{4p-4h} \end{pmatrix}. \quad (8)$$

The parameters  $\Delta_{2p-2h}$  and  $\Delta_{4p-4h}$  are the same as the ones defined in Eq. (3), and the non-diagonal matrix elements  $\Omega_{i,i}$  are the expectation values of  $\hat{V}_{\text{mix},i}$  in the coherent state basis [Eq. (7)]. By substituting the IBM parameters given in Table III and computing the lowest eigenpotential by means

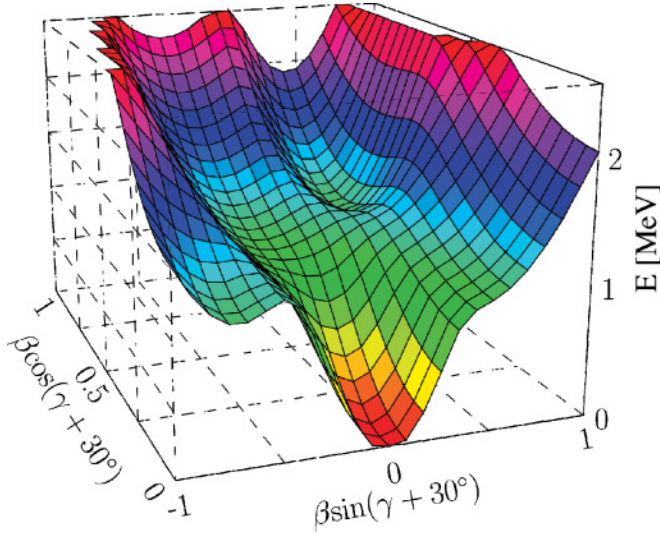


FIG. 18. (Color online) Potential energy surface in  $\beta$  and  $\gamma$  for  $^{186}\text{Pb}$ , constructed using the coherent state approach for the IBM with configuration mixing [90].

of diagonalization, the PES in  $\beta$  and  $\gamma$  for  $^{186}\text{Pb}$  can be obtained (see Fig. 18). Whereas the mixing derived in Ref. [83] resulted in a PES with a spherical and oblate minimum, the mixing parameters determined in this work give rise to three coexisting spherical, oblate, and prolate minima. This result is consistent with the outcome of sophisticated deformed mean-field calculations [15,16].

The same conclusion can be drawn for the values of the deformation parameter  $\beta_0$ . In the IBM, quadrupole moments are calculated as

$$Q(J) = \sqrt{\frac{16\pi}{5}} \langle JJ | T(E2)_0 | JJ \rangle. \quad (9)$$

Assuming a  $K = 0$  band, the collective rotational model delivers the following relation between the quadrupole moment and the deformation parameter  $\beta_0$ :

$$Q = \frac{-J}{2J+3} \frac{3ZR_0^2}{\sqrt{5\pi}} \beta_0. \quad (10)$$

Equating the IBM quadrupole moment for the unperturbed 2p-2h and 4p-4h bands results in deformation parameters that vary between  $-0.14$  and  $-0.16$  for the unperturbed 2p-2h band and between  $0.27$  and  $0.32$  for the unperturbed 4p-4h band. These results are in reasonable agreement with the  $\beta_0$  values obtained in Sec. V A, although the IBM gives slightly smaller values.

## VI. CONCLUSIONS

The present study investigated the structure of the neutron mid-shell nucleus  $^{186}\text{Pb}$  in a recoil-decay tagging experiment for the first time. A backbend in the rotational-like yrast sequence, similar to adjacent Hg and Pt nuclei, was tentatively observed at  $I^\pi = 16^+$ . Besides the yrast band, a non-yrast band starting at  $I^\pi = 2^+$  was observed. The decay pattern to the

yrast band is consistent with results derived from a symmetry-dictated shell-model truncation, the interacting boson model, and it follows that the non-yrast band is dominated by a proton 2p-2h configuration. It has been shown that this structure can be associated with an intrinsic oblate character by analyzing the IBM results within a coherent-state description as well as starting from a microscopic mean-field (HF+BCS+GCM) origin. The observed candidate  $\gamma$  band with odd-spin values, starting at  $I^\pi = 3^+$ , is quite similar to the odd-spin band structure in the nearby  $^{186}\text{Pt}$  nucleus, but more statistics are needed to substantiate such a suggestion. A negative-parity band at still higher energies might be a candidate for part of an octupole band.

The present data were analyzed starting from state-of-the-art mean-field studies using the generator coordinate method in order to handle dynamic effects that go beyond a static mean-field study, as well as starting from a highly truncated shell model in which proton 2p-2h and proton 4p-4h excitations interacting with the valence neutrons are treated as interacting pairs of bosons. Detailed results have been presented on both the resulting bands and their  $E2$  decay properties and have been compared extensively with the new data. The equivalence between the mean-field and IBM approach is discussed, making use of the matrix coherent state method and catastrophe theory to transform the laboratory frame treatment into an intrinsically deformed structure.

Finally, the present data support the interpretation of Andreyev *et al.* [8] as a situation of triple-shape coexistence on the basis of not only the presence of the spherical ground state and two more collective bands that can be associated with a prolate and oblate intrinsic structure, but also of the  $E2$  decay properties when comparing the data and the results of the theoretical calculations. However, more experiments are needed to extract the salient features that go with the unique situation of three close-lying intrinsic structures. Simultaneous in-beam electron and  $\gamma$ -ray spectroscopic studies and lifetime measurements of the low-lying  $0^+$  states will sharpen the understanding of these complex phenomena appearing in the single-closed shell nucleus  $^{186}\text{Pb}$ .

## ACKNOWLEDGMENTS

The UK/France (EPSRC/IN2P3) Loan Pool and EUROBALL Owners Committee is acknowledged for work with the EUROGAM detectors of JuroGam. This work was supported by the EU-FP5-IHP-Access-to-JYFL Project (Contract No. HPRI-CT-1999-00044), the EU-FP5-IHP-RTD-EXOTAG Project (Contract No. HPRI-CT-1999-50017), the Academy of Finland under the Finnish Centre of Excellence Programme 2000-2005 (Project No. 44875), and the EPSRC (UK). Financial support from the FWO-Vlaanderen, the University of Ghent as well as from the OSTC (Grant IUAP #P5/07) is acknowledged (V.H. and K.H.). This research was also supported through a European Community Marie Curie Fellowship (I.G.D.), the Vilho, Yrjö ja Kalle Väisälä Foundation, and the Magnus Ehrnrooth Foundation (J.P.).

- [1] J. L. Wood, K. Heyde, W. Nazarewicz, M. Huyse, and P. Van Duppen, *Phys. Rep.* **215**, 101 (1992).
- [2] P. Van Duppen, E. Coenen, K. Deneffe, M. Huyse, K. Heyde, and P. Van Isacker, *Phys. Rev. Lett.* **52**, 1974 (1984).
- [3] P. Van Duppen, M. Huyse, K. Heyde, and J. L. Wood, *J. Phys. G: Nucl. Part. Phys.* **16**, 441 (1990).
- [4] K. Heyde, J. Schietse, and C. De Coster, *Phys. Rev. C* **44**, 2216 (1991).
- [5] R. Julin, K. Helariutta, and M. Muikku, *J. Phys. G: Nucl. Part. Phys.* **27**, R109 (2001).
- [6] P. Van Duppen, E. Coenen, K. Deneffe, M. Huyse, and J. L. Wood, *Phys. Lett.* **B154**, 354 (1985).
- [7] N. Bijmens *et al.*, *Z. Phys. A* **356**, 3 (1996).
- [8] A. N. Andreyev *et al.*, *Nature (London)* **405**, 430 (2000).
- [9] A. N. Andreyev *et al.*, *Eur. Phys. J. A* **6**, 381 (1999).
- [10] F. R. May, V. V. Pashkewich, and S. Frauendorf, *Phys. Lett.* **B68**, 113 (1977).
- [11] R. Bengtsson and W. Nazarewicz, *Z. Phys. A* **334**, 269 (1989).
- [12] W. Nazarewicz, *Phys. Lett.* **B305**, 195 (1993).
- [13] N. Tajima, P. Bonche, H. Flocard, P.-H. Heenen, and M. S. Weiss, *Nucl. Phys.* **A551**, 409 (1993).
- [14] T. Duguet, M. Bender, P. Bonche, and P.-H. Heenen, *Phys. Lett.* **B559**, 201 (2003).
- [15] M. Bender, P. Bonche, T. Duguet, and P.-H. Heenen, *Phys. Rev. C* **69**, 064303 (2004).
- [16] R. R. Rodríguez-Guzmán, J. L. Egido, and L. M. Robledo, *Phys. Rev. C* **69**, 054319 (2004).
- [17] J. Heese, K. H. Maier, H. Grawe, J. Grebosz, H. Kluge, W. Meczynski, M. Schramm, R. Schubert, K. Spohr, and J. Styczen, *Phys. Lett.* **B302**, 390 (1993).
- [18] A. M. Baxter *et al.*, *Phys. Rev. C* **48**, R2140 (1993).
- [19] W. Reviol, C. J. Chiara, O. Pechenaya, D. G. Sarantites, P. Fallon, and A. O. Macchiavelli, *Phys. Rev. C* **68**, 054317 (2003).
- [20] J. Pakarinen *et al.*, *AIP Conf. Proc.* **831**, 529 (2006).
- [21] J. Pakarinen *et al.*, *Phys. Rev. C* **72**, 011304(R) (2005).
- [22] D. G. Jenkins *et al.*, *Phys. Rev. C* **62**, 021302(R) (2000).
- [23] J. F. C. Cocks *et al.*, *Eur. Phys. J. A* **3**, 17 (1998).
- [24] G. D. Dracoulis, A. P. Byrne, and A. M. Baxter, *Phys. Lett.* **B432**, 37 (1998).
- [25] K. Van de Vel *et al.*, *Eur. Phys. J. A* **17**, 167 (2003).
- [26] R. B. E. Taylor *et al.*, *Phys. Rev. C* **59**, 673 (1999).
- [27] P. Heikkinen and E. Liukkonen, in *Cyclotrons and Their Applications: Proceedings of the 14th International Conference, Cape Town, South Africa 8–13 October 1995*, edited by J. C. Cornell (World Scientific, Singapore, 1996).
- [28] M. Leino *et al.*, *Nucl. Instrum. Methods Phys. Res. B* **99**, 653 (1995).
- [29] R. D. Page *et al.*, *Nucl. Instrum. Methods Phys. Res. B* **204**, 634 (2003).
- [30] C. W. Beausang *et al.*, *Nucl. Instrum. Methods Phys. Res. A* **313**, 37 (1992).
- [31] I. H. Lazarus *et al.*, *IEEE Trans. Nucl. Sci.* **48**, 567 (2001).
- [32] P. Rahkila (2006), <http://trac.cc.jyu.fi/projects/grain>
- [33] D. Radford (2001), <http://radware.phy.ornl.gov/>
- [34] J. Wauters, N. Bijmens, H. Folger, M. Huyse, Han Yull Hwang, R. Kirchner, J. von Schwarzenberg, and P. Van Duppen, *Phys. Rev. C* **50**, 2768 (1994).
- [35] T. Yamazaki, *Nucl. Data A* **3**, 1 (1967).
- [36] E. Der Mateosian and A. W. Sunyar, *At. Data Nucl. Data Tables* **13**, 391 (1974).
- [37] K. S. Krane, R. M. Steffen, and R. M. Wheeler, *Nucl. Data Tables A* **11**, 351 (1973).
- [38] J. Billowes, *Hyperfine Interact.* **30**, 265 (1986).
- [39] G. D. Dracoulis, G. J. Lane, A. P. Byrne, A. M. Baxter, T. Kibédi, A. O. Macchiavelli, P. Fallon, and R. M. Clark, *Phys. Rev. C* **67**, 051301(R) (2003).
- [40] G. D. Dracoulis, G. J. Lane, A. P. Byrne, T. Kibédi, A. M. Baxter, A. O. Macchiavelli, P. Fallon, and R. M. Clark, *Phys. Rev. C* **69**, 054318 (2004).
- [41] J. Penninga, W. H. A. Hesselink, A. Balanda, A. Stolk, H. Verheul, J. van Klinken, H. J. Riezebos, and M. J. A. de Voigt, *Nucl. Phys.* **A471**, 535 (1987).
- [42] D. P. McNabb *et al.*, *Phys. Rev. C* **56**, 2474 (1997).
- [43] B. Fant *et al.*, *J. Phys. G: Nucl. Part. Phys.* **17**, 319 (1991).
- [44] G. Baldsiefen, H. Hubel, W. Korten, U. J. van Severen, J. A. Cizewski, N. H. Medina, D. R. Napoli, C. Rossi Alvarez, G. Lo Bianco, and S. Signorelli, *Z. Phys. A* **355**, 337 (1996).
- [45] A. Görgen *et al.*, *Nucl. Phys.* **A683**, 108 (2001).
- [46] R. J. McDonald and J. E. Draper, *Phys. Rev. C* **17**, 944 (1978).
- [47] H. C. Jain, P. Carlé, A. Källberg, L. O. Norlin, K.-G. Rensfelt, U. Rosengård, and B. Fant, *Nucl. Phys.* **A458**, 225 (2002).
- [48] M. R. Schmorak, *Nucl. Data Sheets* **31**, 283 (1980).
- [49] Ch. Stenzel, H. Grawe, H. Haas, H.-E. Mahnke, and K. H. Maier, *Nucl. Phys.* **A411**, 248 (1983).
- [50] X. Sun, U. Rosengard, H. Grawe, H. Haas, H. Kluge, A. Kuhnert, and K. H. Maier, *Z. Phys. A* **333**, 281 (1989).
- [51] Ch. Stenzel, H. Grawe, H. Haas, H.-E. Mahnke, and K. H. Maier, *Z. Phys. A* **322**, 83 (1985).
- [52] J. J. Van Ruyven, J. Penninga, W. H. A. Hesselink, P. Van Nes, K. Allaart, E. J. Hengeveld, H. Verheul, M. J. A. de Voigt, Z. Sujkowskia, and J. Blomqvist, *Nucl. Phys.* **A471**, 535 (1986).
- [53] F. G. Kondev *et al.*, *Phys. Rev. C* **62**, 044305 (2000).
- [54] K. S. Bindra *et al.*, *Phys. Rev. C* **51**, 401 (1995).
- [55] W. C. Ma, A. V. Ramayya, J. H. Hamilton, S. J. Robinson, J. D. Cole, E. F. Zganjar, E. H. Spejewski, R. Bengtson, W. Nazarewicz, and J.-Y. Zhang, *Phys. Lett.* **B167**, 277 (1986).
- [56] M. J. A. De Voigt, R. Kaczarowski, H. J. Riezebos, R. F. Noorman, J. C. Bacelar, M. A. Deleplanque, R. M. Diamond, F. S. Stephens, J. Sauvage, and B. Roussiére, *Nucl. Phys.* **A507**, 472 (1990).
- [57] R. V. F. Janssens *et al.*, *Phys. Lett.* **B131**, 35 (1983).
- [58] S. M. Harris, *Phys. Rev.* **138**, B509 (1965).
- [59] D. G. Popescu *et al.*, *Phys. Rev. C* **55**, 1175 (1997).
- [60] J. K. Deng *et al.*, *Phys. Rev. C* **52**, 595 (1995).
- [61] W. C. Ma *et al.*, *Phys. Rev. C* **47**, R5 (1993).
- [62] G. Alaga, K. Alder, A. Bohr, and B. R. Mottelson, *Dan. Mat. Fys. Medd.* **29**, 9 (1955).
- [63] K. Helariutta *et al.*, *Eur. Phys. J. A* **6**, 289 (1999).
- [64] J. R. Hughes *et al.*, *Phys. Rev. C* **47**, R1337 (1993).
- [65] J. P. Husson *et al.*, in *Proceedings of the International Conference on Nuclei Far From Stability, Cargese, Corsica, 1976*, CERN Report No. 76-13, 1976 (unpublished).
- [66] M. Finger *et al.*, *Nucl. Phys.* **A188**, 369 (1972).
- [67] K. Heyde and R. A. Meyer, *Phys. Rev. C* **37**, 002170 (1988).
- [68] G. Hebbinghaus, T. Kutsarova, W. Gast, A. Krämer-Flecken, R. M. Lieder, and W. Urban, *Nucl. Phys.* **A514**, 225 (1990).
- [69] J. Kantele, *Handbook of Nuclear Spectroscopy* (Academic, London, 1995).
- [70] G. D. Dracoulis, C. Fahlander, and M. P. Fewell, *Nucl. Phys.* **A383**, 119 (1982).

- [71] B. Cederwall *et al.*, *Z. Phys. A* **337**, 283 (1990).
- [72] F. G. Kondev *et al.*, *Phys. Rev. C* **61**, 044323 (2000).
- [73] R. M. Lieder *et al.*, *Nucl. Phys.* **A645**, 465 (1999).
- [74] G. D. Dracoulis, T. Lännroth, S. Vajda, O. C. Kistner, M. H. Rafailovich, E. Dafni, and G. Schatz, *Phys. Lett.* **B149**, 311 (1984).
- [75] M. Kaci *et al.*, *Nucl. Phys.* **A697**, 3 (2002).
- [76] N. A. Smirnova, P.-H. Heenen, and G. Neyens, *Phys. Lett.* **B569**, 151 (2003).
- [77] G. D. Dracoulis, A. P. Byrne, A. M. Baxter, P. M. Davidson, T. Kibédi, T. R. McGoram, R. A. Bark, and S. M. Mullins, *Phys. Rev. C* **60**, 014303 (1999).
- [78] T. Grahn *et al.*, *Phys. Rev. Lett.* **97**, 062501 (2006).
- [79] K. Heyde, J. Jolie, J. Moreau, J. Ryckebusch, M. Waroquier, P. Van Duppen, M. Huyse, and J. L. Wood, *Nucl. Phys.* **A466**, 189 (1987).
- [80] J. L. Egido, L. M. Robledo, and R. R. Rodríguez-Guzmán, *Phys. Rev. Lett.* **93**, 082502 (2004).
- [81] P. D. Duval and B. R. Barrett, *Nucl. Phys.* **A376**, 213 (1982).
- [82] V. Hellemans, R. Fossion, S. D. Baerdemacker, and K. Heyde, *Phys. Rev. C* **71**, 034308 (2005).
- [83] R. Fossion, K. Heyde, G. Thiamova, and P. Van Isacker, *Phys. Rev. C* **67**, 024306 (2003).
- [84] C. De Coster, K. Heyde, B. Delcroix, P. Van Isacker, J. Jolie, H. Lehman, and J. L. Wood, *Nucl. Phys.* **A600**, 251 (1996).
- [85] R. D. Page *et al.*, in *Proceedings of the Third International Conference on Exotic Nuclei and Atomic Masses ENAM2001, Hämeenlinna, Finland, 2–7 July 2001*, edited by J. Äystä, P. Dendooven, A. Jokinen, and M. Leino (Springer-Verlag, Berlin, 2001), p. 309.
- [86] J. N. Ginocchio and M. W. Kirson, *Phys. Rev. Lett.* **44**, 1744 (1980).
- [87] A. E. L. Dieperink, O. Scholten, and F. Iachello, *Phys. Lett.* **B44**, 1747 (1980).
- [88] A. Bohr and B. R. Mottelson, *Phys. Scr.* **22**, 468 (1980).
- [89] E. López-Moreno and O. Castaños, *Phys. Rev. C* **54**, 2374 (1996).
- [90] A. Frank, P. Van Isacker, and C. E. Vargas, *Phys. Rev. C* **69**, 034323 (2004).